

Boundary-induced transitions in Möbius quenches of holographic BCFT

Alice Bernamonti^{*,*}, Federico Galli^{*}, Dongsheng Ge[†]

^{}Dipartimento di Fisica e Astronomia, Università di Firenze;
Via G. Sansone 1; I-50019 Sesto Fiorentino, Italy*

^{}INFN, Sezione di Firenze;
Via G. Sansone 1; I-50019 Sesto Fiorentino, Italy*

*[†]Department of Physics, Osaka University,
Machikaneyama-Cho 1-1, Toyonaka 560-0043, Japan*

Abstract

Boundary effects play an interesting role in finite-size physical systems. In this work, we study the boundary-induced properties of 1+1-dimensional critical systems driven by inhomogeneous Möbius-like quenches. We focus on the entanglement entropy in BCFTs with a large central charge and a sparse spectrum of low-dimensional operators. We find that the choice of boundary conditions leads to different scenarios of dynamical phase transitions. We also derive these results in a holographic description in terms of intersecting branes in AdS₃, and find a precise match.

Contents

1	Introduction	2
2	BCFT with mixed boundary conditions	6
2.1	Strip with mixed boundary conditions	7
2.2	Twist operator correlator	8
2.3	Universal contribution from the stress tensor	10
3	Entanglement entropy evolution under SSD and Möbius Hamiltonians	13
3.1	SSD and Möbius Hamiltonian on the strip	14
3.2	Entanglement entropy after the quench	16
4	Quench with generally deformed Hamiltonians	26
4.1	A general class of deformed Hamiltonians	26
4.2	Entanglement entropy after the quench	27
5	Holographic dual	31
5.1	Gravitational action and equations of motion	32
5.2	Intersecting branes in AdS_3	34
5.3	Holographic entanglement entropy	36
6	Discussion	41
A	Stress tensor in the UHP	46

1 Introduction

Ordinary physical systems have boundaries. These introduce boundary effects, which can be probed by physical quantities, such as the partition and correlation functions. Of particular interest are conformally invariant systems with conformal boundaries, described by boundary conformal field theory (BCFT). In 1+1 dimensions this subject was mainly laid out by Cardy [1–3], and it is the main focus of this work.

In 2d BCFT, boundary effects are captured by the boundary entropy $s_{\mathcal{B}} = \ln g_{\mathcal{B}} \equiv \ln \langle 0 | \mathcal{B} \rangle$, which measures the ground state degeneracy for a given conformal boundary condition \mathcal{B} [4–6]. This can be evaluated explicitly in rational conformal field theories once the solutions to Cardy’s equation are found [1, 7, 8]. For an infinite strip of width

L , the boundary conditions for its two edges can be chosen differently. As a result, the distinct boundary conditions lead to two different boundary entropies. In rational CFT they can assume a limited number of values due to the presence of a finite number of boundary primaries [8].

Here we are concerned mainly with holographic CFTs, which have a large central charge c and a sparse spectrum of light operators [9, 10]. Large part of the recent work in holographic BCFT is connected with the developments in understanding entanglement in gravitational systems, via the entanglement island proposal [11–15]. This has sparked renewed interest in refining the understanding of the AdS/BCFT correspondence [16, 17]. In the simplest AdS/BCFT models, boundary conditions are implemented via the insertion of end of the world (EOW) branes anchored on the spacetime boundary and extending into the AdS bulk [16, 17]. A number of features emerge for holographic BCFTs realized in this way [16–27]. In particular, they have a continuous spectrum of heavy operators, with conformal weight proportional to the central charge, up to the black hole threshold $c/24$. Also, the tension T_i of the EOW branes in the AdS bulk determines the boundary entropy $s_i = \frac{c}{6} \operatorname{arctanh} T_i$ for the dual boundary state [16, 17]. The brane tension can take values continuously in the range $|T_i| \leq 1$ and thus yields for these models a boundary entropy taking arbitrary values and scaling with the CFT central charge. Indeed, in the holographic computation of the entanglement entropy in AdS/BCFT models, the boundary entropy arises from the Ryu-Takayanagi formula applied to bulk geometries bounded by EOW branes [16, 17].

In holographic BCFT, different competing phases in the evaluation of the entanglement entropy may arise, and the boundary entropy plays a role in determining the dominant one. These situations include holographic computations in terms of the Ryu-Takayanagi surfaces [16, 17], but also first principles CFT calculations in specific limits, and applications to double holographic models via the entanglement island formula as in, *e.g.*, [11–14, 23, 26, 28, 29].

In far-from-equilibrium settings, such as those generated by quantum quenches, the system may experience dynamical transitions between these competing phases. In this work, we consider spatially inhomogeneous quenches in 2d BCFT. In particular, we focus on a family of processes in which the Hamiltonian is abruptly changed to the so called Möbius Hamiltonian [30–38]. A well-studied limit of this class is known as sine-square-deformed (SSD) Hamiltonian, which was originally introduced to suppress boundary effects and efficiently isolate bulk properties [30–33, 39–41]. In fact, it was observed that in 1+1-dimensional CFT the SSD Hamiltonian shares the same ground state of a uniform system with periodic boundary conditions and that, to a certain

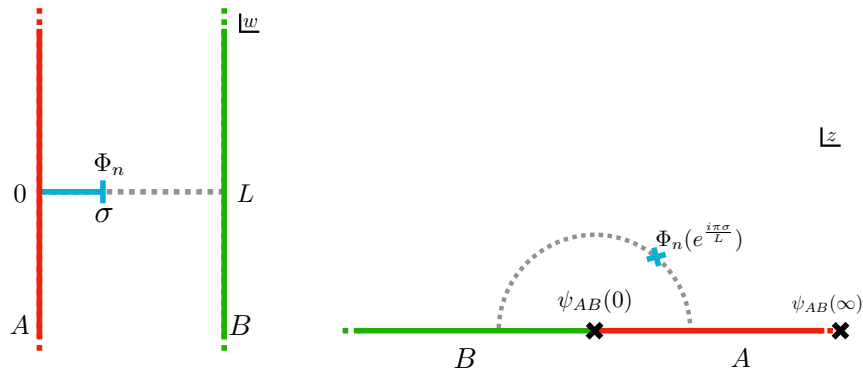


Figure 1: Left: The physical system is defined on a strip of spatial width L , with conformal boundary conditions A and B at the two edges. We consider a bipartition of the system defined considering a spatial interval of size σ adjacent to the boundary with conformal boundary condition A . Via the replica trick the evaluation of the entanglement entropy for this bipartition is mapped to calculating the one point function of a replica twist operator Φ_n inserted at the endpoint of the interval. Right: The system mapped to the upper half plane. The change in boundary conditions is sustained by the insertion of a boundary condition changing operator ψ_{AB} .

extent, the system size is effectively infinite in this limit [34, 35, 42–44].

As we summarize below, here we deal with an instance that combines the above ingredients. For a BCFT on an interval with mixed boundary conditions, we study the entanglement entropy evolution following an inhomogeneous quench by a Möbius-like deformation. We will show that two competing phases in the entanglement entropy arise from the presence of mixed boundary conditions, and that a dynamical transition from one phase to the other is controlled by the quench protocol. This is a new feature as compared to previous studies on this class of quenches, where boundary effects were found to be suppressed [30–34].

Summary

The dynamical process we consider is the following. We prepare a state $|\psi_{AB}\rangle$ on a finite-size system of length L , with distinct boundary conditions A and B , as illustrated in fig. 1. This is achieved inserting boundary condition changing (BCC) operators, which mediate the change in boundary conditions [45]. BCC operators are not local operators of the boundary CFT in the conventional sense, but are treated as boundary primaries with similar scaling properties as bulk primaries [3]. In particular $|\psi_{AB}\rangle$ can be seen as an eigenstate of the BCFT Hamiltonian.

At $t = 0$ the state is quenched by turning on a deformation of the BCFT Hamiltonian. For $t > 0$ the system is driven with such a deformed Hamiltonian and undergoes a non-trivial evolution.¹ We analyse the dynamics following from different deformations: the SSD, Möbius and generalized deformation of section 4. A key technical advantage is that these allow to explicitly obtain the time evolution in a closed form [34, 35, 47].

As a probe of the dynamics, we consider the real-time evolution of the entanglement entropy for an interval adjacent to one end of the system. Via the replica trick, the computation of the entanglement entropy is recast in evaluating a three-point function of two BCC operators and a replica twist in the bulk. The details of such a correlator depend on the specific theory. We extract and analyse the contribution coming from the conformal family of the stress tensor. The reason is twofold. On the one hand, this contribution is universal. It is present in every 2d CFT with the identity operator in its normalizable spectrum, and it does not depend on CFT data other than the central charge and the ground state degeneracy. On the other hand, in holographic CFTs the contribution of the identity conformal family is expected to dominate, and to match dual holographic calculations in three dimensional semiclassical gravity.

With mixed boundary conditions the approximate result obtained from the conformal family of the identity operator is not unique. There are different boundary operator expansions of a bulk CFT operator one can consider [48]. In particular, one associated with boundary condition A and one with boundary condition B . These give competing channels in the evaluation of the correlator. Already in the initial state what channel, or phase, dominates depends on the size of the interval considered and difference in boundary entropies $s_{A,B}$ [21–23]. More interestingly, we show that the quench dynamics can drive a transition from one phase to the other (and back) as time evolves.

We find that the dynamical phase transition pattern is determined by the relative amount of boundary degrees of freedom associated to the two boundaries. Depending on the difference between s_A and s_B , the entanglement entropy can exhibit or not a transition between phase A and phase B . Under the SSD dynamics the transition can only happen once, while it becomes recurrent for the Möbius-like quenches, with characteristic timescales determined by the details of the deformation.

This finds an exact match and a simple interpretation in the holographic gravitational bulk description obtained in terms of AdS_3 bounded by two intersecting EOW branes [21, 22]. We show that the entanglement entropy obtained in the BCFT com-

¹In spirit, this is the same thing happening in the prototypical global quench protocol of Calabrese and Cardy [46]. In both cases the initial state is not an eigenstate of the Hamiltonian that drives the dynamics for $t > 0$.

putation for the two phases is in one to one correspondence with the length of minimal geodesics. Indeed for a point on the AdS_3 boundary, there exists in general two competing Ryu-Takayanagi geodesics, each ending on one of the two EOW branes. We also show that the entanglement dynamics can be matched exploiting the local equivalence of AdS_3 geometries and extending the map relating the initial and time evolved state in the BCFT to a diffeomorphism in the bulk.

The rest of the paper is organized as follows, in section 2, we introduce the setup and relevant BCFT technicalities needed for our analysis. In particular, we show how the initial state of our system is defined and compute the corresponding entanglement entropy. In section 3, we introduce the SSD and Möbius Hamiltonian on the strip, and analyze the time evolution of the entanglement entropy for a quench with these Hamiltonians. In section 4, we consider the generalization of this analysis to the case of deformed Hamiltonians obtained from $sl(2, \mathbb{R})$ subalgebras of Virasoro generators at arbitrary levels. Section 5 describes the holographic dual of our setup and analysis. Using a bulk description in terms of AdS_3 with intersecting EOW branes, we find an exact match of the BCFT computation with the holographic result. We conclude in section 6, where we comment on the broader applicability of our analysis and results, and give future perspectives.

2 BCFT with mixed boundary conditions

In this section we review how to characterize a CFT on an interval with different conformal boundary conditions, A and B , at the two ends [3, 45, 48]. The state with mixed boundary conditions we will consider, $|\psi_{AB}\rangle$, will either be the ground state or a high energy eigenstate for the BCFT with distinct boundary conditions.

We will review how to evaluate the entanglement entropy in this state for an interval adjacent to one of the boundaries. Via the replica approach, this reduces to evaluating a replica twist one-point function on the strip with mixed boundary conditions. Specializing to the case of holographic CFTs, we will approximate the correlator with the universal contribution of the stress tensor and its conformal family. This is motivated by the assumptions in an holographic CFT on the sparseness of the spectrum of low dimensional operators and on the dominance of the identity Virasoro conformal block (see, *e.g.*, [9, 10, 49–56] for examples and discussions). Let us remark that this is a working assumption and here we are not proving the validity of this approximation. We will however show explicitly in section 5 that the result obtained in this way ex-

actly captures the result following from the corresponding dual computation in terms of Ryu-Takayanagi surfaces [16, 17, 57, 58].

2.1 Strip with mixed boundary conditions

We consider a state in a CFT on an interval with two different conformally invariant boundary conditions. In particular, in the Euclidean plane $w = \tau + i\sigma$, we consider an infinite strip $-\infty < \tau < \infty$ of width $0 \leq \sigma \leq L$. Two conformally invariant boundary conditions A, B are imposed along $\sigma = 0$ and $\sigma = L$ respectively. With

$$z = e^{\frac{\pi}{L}w} \quad (2.1)$$

the strip is mapped into the upper half plane (UHP), with the two boundaries $\sigma = 0, L$ mapped respectively to the positive and negative real axis $z = x$. In the UHP the change in conformal boundary conditions along the boundary at $x = 0, \infty$ is mediated by boundary condition changing (BCC) operators $\psi_{AB}(x)$ (see fig. 1) [3, 48]. More precisely, starting in the UHP with a state with homogeneous boundary condition A , the mixed boundary conditions A and B state is obtained as²

$$|\psi_{AB}\rangle = \psi_{AB}(0) |0\rangle_{AA} \quad \langle\psi_{AB}| = \lim_{x \rightarrow \infty} \frac{x^{2h_\psi}}{c_{\psi\psi}} {}_{AA}\langle 0| \psi_{AB}(x) \equiv {}_{AA}\langle 0| \psi_{AB}(\infty). \quad (2.2)$$

BCC operators act non-locally to implement the change of boundary conditions, but can be treated as primaries with weight h_ψ in the CFT defined on the boundary [3, 48]. $c_{\psi\psi}$ is the coefficient of the two-point function of the BCC operator, so that the state is normalized $\langle\psi_{AB}|\psi_{AB}\rangle = 1$. The conformal dimension h_ψ is determined in terms of gap in energy between the initial state, with homogeneous boundary conditions A , and the state with mixed boundary conditions A and B . In particular [45]

$$h_\psi = \frac{L \Delta E}{\pi} = \frac{L}{\pi} (E_{AB} - E_{AA}), \quad (2.3)$$

where E_{AA} is the energy of the ground state on the strip with boundary conditions A . E_{AB} instead is the energy of the lowest energy eigenstate on the strip with mixed boundary conditions with a non-zero overlap with $|\psi_{AB}\rangle$. Notice that depending on the operator ψ_{AB} , this may correspond to the ground state or an excited state of the BCFT with mixed boundary conditions [45].

We are interested in holographic BCFTs, which have a dual description in terms of semiclassical gravitational configurations in AdS_3 . For these, the change in boundary

²For notational simplicity and since it is clear from the context, we do not distinguish between the BCC operators ψ_{AB} and ψ_{BA} [48].

conditions holographically translates into a change of the asymptotically AdS_3 geometry [16, 17, 59]. The corresponding change in energy is thus proportional to the central charge c . We will then be concerned with the case where the BCC has a conformal weight proportional to the central charge c of the BCFT [21–23]. As we will review in section 5, in bottom-up models of holographic CFTs the BCC conformal operators have a continuous spectrum in the range $0 < h_\psi/c \leq 1/24$ [21, 22]. When talking of holographic BCFT in the rest of this work we will then assume implicitly this range of values.

2.2 Twist operator correlator

We want to evaluate the entanglement entropy for a spatial region consisting of a portion of the strip that includes one of the boundaries. Without loss of generality, we pick the entangling region to be a portion of dimension $0 < \sigma < L$ of the entire system, adjacent to the origin. The boundary included in this region is therefore the one with boundary condition A , see fig. 1.

Using the replica trick, the entanglement entropy S can be obtained in terms of the Rényi entropies $S_\sigma^{(n)}$ (for a review see [6]). For any integer $n \geq 2$, these are defined from the reduced density matrix ρ_σ associated to the geometric region we are considering as

$$S_\sigma^{(n)} = \frac{1}{1-n} \log \text{Tr} \rho_\sigma^n. \quad (2.4)$$

The computation of $S_\sigma^{(n)}$ can be recast into the evaluation of a correlator of twist operators in the strip geometry with mixed boundary conditions. For the case at hand this is a one-point function³

$$S_\sigma^{(n)} = \frac{1}{1-n} \log \langle \psi_{AB} | \Phi_n(w = i\sigma, \bar{w} = -i\sigma) | \psi_{AB} \rangle, \quad (2.5)$$

with the twist operator Φ_n inserted at the endpoint of the entangling interval (see fig. 1). The entanglement entropy S is then obtained as the analytic continuation to $n = 1$. Schematically,

$$S = \lim_{n \rightarrow 1} S_\sigma^{(n)} = \lim_{n \rightarrow 1} \frac{1}{1-n} \log \langle \psi_{AB} | \Phi_n(w, \bar{w}) | \psi_{AB} \rangle. \quad (2.6)$$

The above correlator is not defined in the original CFT, but in the cyclic orbifold theory $\text{CFT}^n/\mathbb{Z}_n$ resulting from using the replica trick.⁴ The corresponding replica

³Here are considering a time independent state, so we are setting $\tau = 0$ without loss of generality.

⁴In defining the state $|\psi_{AB}\rangle$ in (2.5) one would actually need to consider the operator $\Psi_{AB} = \psi_{AB}^{\otimes n}$ in the orbifold $\text{CFT}^n/\mathbb{Z}_n$, instead of ψ_{AB} . Nonetheless, for all practical purposes, in the limit (2.6) one can simply keep defining the state with ψ_{AB} . Any appearance of Ψ_{AB} via $h_\Psi = nh_\psi$ would reduce to the effect of having ψ_{AB} with h_ψ . See, *e.g.*, [29, 52] for similar computations.

twist field has conformal dimension

$$h_h = \bar{h}_n = \frac{c}{24} \left(n - \frac{1}{n} \right). \quad (2.7)$$

The strip correlator on the right hand side of (2.6) is conveniently evaluated via a map to the UHP. Using $z = e^{\frac{\pi}{L}w}$ and owing to the normalization of the state we have⁵

$$\langle \psi_{AB} | \Phi_n(w, \bar{w}) | \psi_{AB} \rangle = \left(\frac{\partial z}{\partial w} \right)^{h_n} \left(\frac{\partial \bar{z}}{\partial \bar{w}} \right)^{h_n} \langle \psi_{AB}(0) \Phi_n(z, \bar{z}) \psi_{AB}(\infty) \rangle_{\text{UHP}}. \quad (2.8)$$

This three point function in the UHP involves two boundary and one bulk operator and is thus not completely fixed by conformal invariance. Similarly to a four-point function in the full complex plane, it can be expanded in the sum of conformal Virasoro blocks. There are in fact two different expansions, or channels, one can consider here [48]. One can perform the boundary expansion of a primary bulk operator Φ , in our case a bulk twist operator, assuming it approaches the boundary where the boundary condition is fixed to be A . Alternatively, Φ can be expanded in terms of boundary operators assuming the condition on the boundary is B . The two corresponding conformal block expansions can be written as [48]

$$\langle \psi_{AB}(0) \Phi(z, \bar{z}) \psi_{AB}(\infty) \rangle_{\text{UHP}} = (z - \bar{z})^{-2h_\Phi} (1 - \eta)^{2h_\Phi} \sum_p C_p^A \mathcal{F}_p(1 - \eta), \quad (2.9)$$

and

$$\langle \psi_{AB}(0) \Phi(z, \bar{z}) \psi_{AB}(\infty) \rangle_{\text{UHP}} = (z - \bar{z})^{-2h_\Phi} (1 - \eta)^{2h_\Phi} \sum_p C_p^B \mathcal{F}_p(1 - e^{-2\pi i} \eta) \quad (2.10)$$

where we defined the ratio

$$\eta = \frac{z}{\bar{z}}. \quad (2.11)$$

In the above expressions, the sum is over exchanged primaries of the CFT defined on the boundary, with C_p^A and C_p^B constants related to operator expansion coefficients (see [48] for details). \mathcal{F}_p is the same function defining the holomorphic Virasoro conformal block in the full complex plane. More precisely, take in the full complex plane a primary ϕ having the same conformal weight as Φ and a primary ψ with the same conformal weight as ψ_{AB} . $\mathcal{F}_p(1 - \eta)$ is then the holomorphic Virasoro conformal block appearing in the t-channel expansion

$$\langle \psi(0) \phi(\eta, \bar{\eta}) \phi(1) \psi(\infty) \rangle_{\text{plane}} = \sum_p a_p \mathcal{F}_p(1 - \eta) \bar{\mathcal{F}}_p(1 - \bar{\eta}). \quad (2.12)$$

⁵The UHP expectation value is homogeneous with uniform boundary condition A , that is $\langle \dots \rangle_{\text{UHP}} = {}_{AA} \langle 0 | \dots | 0 \rangle_{AA}$.

Notice that despite the full correlator being single valued in the complex plane, \mathcal{F}_p is in general multivalued in the η plane and requires a choice of branch cut. Here we are taking the branch cut of $\mathcal{F}_p(1 - \eta)$ in such a way as to recover the expected short distance singularity in the OPE limit $\phi(\eta, \bar{\eta}) \rightarrow \phi(1)$. Having fixed that, the explicit phase in front of η in (2.10) differentiates the single terms in the expansion from those in (2.9). Of course, the exact correlator obtained from the full sums is single valued.

As discussed in section 2.1, we will consider the case of heavy BCC operators ψ_{AB} with conformal weight h_ψ scaling with the central charge c . In our computation the bulk operator above is identified with a replica twist Φ_n . Its weight h_n also scales with the central charge of the CFT, but $h_n/c \rightarrow 0$ in the limit $n \rightarrow 1$. In the holographic CFT literature this is referred to as a (perturbatively) light operator (see, *e.g.*, [50, 55]). The relevant Virasoro conformal blocks \mathcal{F}_p are therefore those for an Heavy-Heavy-Light-Light four point function (2.12). At the leading order in a large c expansion these are known in a closed form [50, 55].

2.3 Universal contribution from the stress tensor

The two expansions (2.9) and (2.10) give completely equivalent results when evaluating the full correlator $\langle \psi(0) \Phi_n(z, \bar{z}) \psi(\infty) \rangle_{\text{UHP}}$. However, for holographic CFTs the full CFT data are not known and we can only provide an approximate result. We will consider the universal contribution of the stress tensor coming from the identity Virasoro block and assume that in an holographic CFT the correlator is well approximated by this contribution alone (see, *e.g.*, [49–53, 55, 56] for work in similar context and more detailed discussions of this approximation).

Roughly speaking, this approximation is motivated by the fact that for holographic CFTs the sum over Virasoro conformal blocks is a sum of exponentials, weighted by the conformal dimension of the exchanged operator [60, 61]. Applying a saddle-point approach, the sum is then approximated by the largest term. For holographic CFTs, which have a sparse spectrum of low-dimensional operators, this is given by the identity Virasoro block. In making this approximation one is also assuming that other contributions from light operators are suppressed in the large c expansion, and ignoring possible non-perturbative terms. In addition, the universal contribution of the stress energy tensor alone is expected to encode the geometric features of the dual holographic description, as we will show in section 5.

The different expansions channels in (2.9) and (2.10) provide competing identity Virasoro block approximations. Following the saddle point logic, one is then lead to consider these channels as competing, and to retain the dominant saddle point contri-

bution. Here we shall notice that we expect each of the identity Virasoro contributions to provide a good approximation to the full correlator only for some range of the parameters. When knowing the full correlator one would observe a smooth transition connecting these regimes [62]. In our working approach, where we only retain two competing saddles provided by the identity Virasoro block, we will instead observe a sharp transition.

To evaluate the correlator, we then consider the explicit expression for the Virasoro identity block at leading order in a large c expansion [50, 55]

$$\mathcal{F}_0(1 - \eta) = \eta^{(\alpha-1)h_n} \left(\frac{1 - \eta^\alpha}{\alpha} \right)^{-2h_n}. \quad (2.13)$$

Here

$$\alpha = \sqrt{1 - \frac{24h_\psi}{c}}, \quad (2.14)$$

and h_n is the conformal weight (2.7) of the twist operator Φ_n . Notice that (2.13) is only valid for $h_n/c \ll 1$, *i.e.*, for n close to one.

At leading order in the $\eta \rightarrow 1$ limit

$$\mathcal{F}_0(1 - \eta) \approx (1 - \eta)^{-2h_n}. \quad (2.15)$$

Taking this limit in (2.9) selects the identity contribution in the bulk to boundary OPE of the bulk operator Φ_n . This shows how the coefficient C_0^A in (2.9) is related to the expectation value of Φ_n in the UHP with homogeneous boundary conditions A . Explicitly

$$\langle \Phi_n(z, \bar{z}) \rangle_{\text{UHP}} = \frac{A_{\Phi_n}}{|z - \bar{z}|^{2h_n}} = \frac{C_0^A}{(z - \bar{z})^{2h_n}}, \quad (2.16)$$

where we are neglecting the regularization associated to the insertion of a twist operator, which will be restored in the final result for the entanglement entropy.

Approximating the full three-point function with the identity contribution in the A -channel (2.9) then gives

$$\begin{aligned} \langle \psi_{AB} | \Phi_n(z, \bar{z}) | \psi_{AB} \rangle_{\text{UHP}} &\approx C_0^A \alpha^{2h_n} (z\bar{z})^{(\alpha-1)h_n} (z^\alpha - \bar{z}^\alpha)^{-2h_n} \\ &= C_0^A \alpha^{2h_n} (z\bar{z})^{-h_n} \left[2 \sinh \frac{\alpha}{2} \log \frac{z}{\bar{z}} \right]^{-2h_n}, \end{aligned} \quad (2.17)$$

which via (2.8) in terms of the physical strip setup yields

$$\langle \psi_{AB} | \Phi_n(w, \bar{w}) | \psi_{AB} \rangle \approx A_{\Phi_n} \left(\frac{\alpha\pi}{2L} \right)^{2h_n} \left[\sin \alpha\pi \frac{\sigma}{L} \right]^{-2h_n}. \quad (2.18)$$

In the last expression we have used the fact that the twist insertion is at $w = i\sigma$. In the limit $\sigma \rightarrow 0$ this result reproduces the result for a small entangling region adjacent to the boundary at $\sigma = 0$ [6], which is insensitive to boundary condition B .

Performing the same computation for the expansion in the B -channel (2.10) gives

$$\langle \psi_{AB} | \Phi_n(z, \bar{z}) | \psi_{AB} \rangle_{\text{UHP}} \approx C_0^B \alpha^{2h_n} (z\bar{z})^{-h_n} \left[2 \sinh \frac{\alpha}{2} \left(\log \frac{z}{\bar{z}} - 2\pi i \right) \right]^{-2h_n}. \quad (2.19)$$

The coefficient C_0^B , up to a phase, is the expectation value B_{Φ_n} of Φ_n in the UHP with boundary conditions B [48]. More precisely, mapping to the strip

$$\langle \psi_{AB} | \Phi_n(w, \bar{w}) | \psi_{AB} \rangle \approx B_{\Phi_n} \left(\frac{\alpha\pi}{2L} \right)^{2h_n} \left[\sin \alpha\pi \frac{L - \sigma}{L} \right]^{-2h_n}. \quad (2.20)$$

Here for $\sigma \rightarrow L$ one recognises the result for a small entangling region adjacent to the boundary at $\sigma = L$ with boundary conditions B [6].

The correlator is then evaluated taking the largest between the approximate results (2.18) and (2.20), which yields

$$\langle \psi_{AB} | \Phi_n(w, \bar{w}) | \psi_{AB} \rangle = \left(\frac{\alpha\pi}{2L} \right)^{2h_n} \max \left\{ A_{\Phi_n} \left[\sin \alpha\pi \frac{\sigma}{L} \right]^{-2h_n}; B_{\Phi_n} \left[\sin \alpha\pi \frac{L - \sigma}{L} \right]^{-2h_n} \right\}. \quad (2.21)$$

Substituting into (2.6) and continuing the result to $n = 1$ gives the entanglement entropy. The maximization in equation (2.21) translates into a minimization over entanglement entropy contributions computed using the two channels

$$S = \frac{c}{6} \log \frac{2L}{\pi\alpha\epsilon} + \min \left\{ \frac{c}{6} \log \sin \frac{\alpha\pi\sigma}{L} + s_A; \frac{c}{6} \log \sin \frac{\alpha\pi(L - \sigma)}{L} + s_B \right\}. \quad (2.22)$$

In writing this result we have made explicit the UV regulator ϵ associated with the insertion of a replica twist operator Φ_n . s_A is the boundary entropy associated to the boundary with boundary conditions A [4–6]

$$s_A \equiv \log g_A = \lim_{n \rightarrow 1} \frac{1}{n-1} \log A_{\Phi_n}, \quad (2.23)$$

and a similar definition holds for s_B . Here $g_{A,B}$ is the ground-state degeneracy of the corresponding boundary condition A, B as defined in [4]. Notice that the boundary entropy $s_{A,B}$ can be both positive or negative. In the holographic realisation of BCFTs it actually takes continuous values in the reals [16, 17] (see also the discussion in sec. 5).

The result in (2.22) reproduces what found in [23] using a map to the twisted UHP where the effect of the stress energy tensor is trivialized. The case with homogeneous boundary condition A and no BCC insertions [47] is recovered for $s_A = s_B$ and $\alpha = 1$. In this limit the two contributions coincide. Indeed, the correlator reduces to the twist operator one point function with boundary condition A , which is fixed by conformal invariance. Taking $s_A = s_B$ and $0 < \alpha < 1$ in (2.22) can be regarded as the case

of a high energy eigenstates on the strip with homogeneous boundary condition A . This is an excited state prepared by the insertion of a primary boundary operator ψ , rather than a BCC. The conformal weight h_ψ corresponds to the energy gap between this excited state and the ground state with homogeneous boundary conditions A . For this state, the exchange of dominance between the two contributions as the size of the interval is changed happens at $\sigma = L/2$.

We are interested in the general case where $s_A \neq s_B$, and in holographic CFTs. For these the boundary entropy scales like the central charge, $s_{A,B} \sim c$ and $0 < h_\psi/c \leq 1/24$ giving $0 < \alpha \leq 1$ [21, 22]. The dominant channel is then determined by the boundary conditions A and B both via the boundary entropy $s_{A,B}$ and the specific state, through the energy gap (2.3) encoded in α . In particular, as the size σ of the interval adjacent to A is increased, S undergoes a transition from channel A to channel B when

$$s_B - s_A = \frac{c}{6} \log \frac{\sin\left(\frac{\alpha\pi\sigma}{L}\right)}{\sin\left(\frac{\alpha\pi(L-\sigma)}{L}\right)}. \quad (2.24)$$

This happens for any boundary state with $s_A \neq s_B$ and for any value $0 < \alpha < 1$. Notice that the transition can happen for arbitrary small values of σ . That is, channel B can become dominant for $\sigma/L \ll 1$ as long as $s_B - s_A$ takes a large negative value. Similarly, for $s_B - s_A$ positive and sufficiently large one can remain in channel A for $(L - \sigma)/L \ll 1$.

3 Entanglement entropy evolution under SSD and Möbius Hamiltonians

In the previous section we described the initial state of our system and the corresponding entanglement entropy computation. We now turn to the study of a particular class of quantum quenches.

A quench is a sudden change in the system that produces a time-dependent excited state. Depending on the protocol, the change can affect the system locally or globally, homogeneously or inhomogeneously. Here we will focus on a class of inhomogeneous quenches that affect the system globally (for other studies on the topic see, *e.g.*, [36–38, 63–73]). They are obtained evolving the initial state with a class of Hamiltonians known as sine-square-deformed (SSD) and Möbius Hamiltonians [30–35]. These are deformations of the usual Hamiltonian of the CFT defined on the strip, H_0 . The state $|\psi_{AB}\rangle$ is an eigenstate of H_0 and represents an out-of-equilibrium state for the evolution dictated by these deformed Hamiltonians.

3.1 SSD and Möbius Hamiltonian on the strip

The SSD Hamiltonian consists of an inhomogeneous spatial deformation of the standard Hamiltonian with a sine squared enveloping function [47]

$$H_{\text{SSD}} \equiv \int_0^L d\sigma \, 2 \sin^2 \left(\frac{\pi \sigma}{L} \right) T_{\tau\tau}(\sigma). \quad (3.1)$$

This can be expressed as

$$H_{\text{SSD}} = H_0 - \frac{1}{2} (H_+ + H_-) \quad (3.2)$$

where

$$H_0 = \int_0^L d\sigma \, T_{\tau\tau}(\sigma) = \int_0^L \frac{dw}{2\pi} (T(w) + \bar{T}(\bar{w})) \quad (3.3)$$

is the standard CFT Hamiltonian on the strip, and the deformations H_{\pm} are defined as

$$H_{\pm} = \int_0^L \frac{dw}{2\pi} \left(e^{\pm 2\pi w/L} T(w) + e^{\mp 2\pi \bar{w}/L} \bar{T}(\bar{w}) \right). \quad (3.4)$$

The Möbius Hamiltonian generalizes this to a one parameter family of deformations

$$H_{\theta} \equiv H_0 - \frac{\tanh(2\theta)}{2} (H_+ + H_-), \quad (3.5)$$

where the SSD Hamiltonian is recovered for $\theta \rightarrow \infty$.

Mapping the strip to the UHP by $z = e^{\frac{\pi w}{L}}$ and using the properties of the stress tensor of a CFT in the UHP [3], one can write

$$\begin{aligned} H_0 &= \frac{\pi}{L} \oint z T(z) - \frac{\pi}{L} \frac{c}{24} = \frac{\pi}{L} \left(L_0 - \frac{c}{24} \right), \\ H_+ + H_- &= \frac{\pi}{L} \oint (z^3 T(z) + z^{-1} T(z)) = \frac{\pi}{L} (L_2 + L_{-2}), \end{aligned} \quad (3.6)$$

with the contour integral defined in the full complex plane (see appendix A for details).

Next to the dilatation generator L_0 , which defines with the Casimir energy the standard Hamiltonian, H_{θ} involves the level-two Virasoro generators $L_{\pm 2}$. The subset $\{L_0, L_{\pm 2}\}$ forms a closed $sl(2, \mathbb{R})$ algebra [74, 75]. It is possible to write in an explicit closed form the action of the Möbius Hamiltonian H_{θ} on a primary operator \mathcal{O} [34, 35, 47]. Its Heisenberg evolution can be expressed as a conformal transformation to new coordinates (z_{t_E}, \bar{z}_{t_E}) such that

$$\mathcal{O}_{t_E}(z, \bar{z}) \equiv e^{H_{\theta} t_E} \mathcal{O}(z, \bar{z}) e^{-H_{\theta} t_E} = \left(\frac{\partial z_{t_E}}{\partial z} \right)^{h_{\mathcal{O}}} \left(\frac{\partial \bar{z}_{t_E}}{\partial \bar{z}} \right)^{\bar{h}_{\mathcal{O}}} \mathcal{O}(z_{t_E}, \bar{z}_{t_E}). \quad (3.7)$$

The explicit form of the transformation can be obtained finding a map to a geometry where H_θ has a simple action [34, 35, 47]. Using

$$\tilde{z}^2 = -\frac{z^2 \cosh \theta - \sinh \theta}{z^2 \sinh \theta - \cosh \theta} \quad (3.8)$$

and a similar one for the \bar{z} coordinate, one gets to

$$\begin{aligned} H_\theta &= \frac{\pi}{L} \left[\frac{1}{\cosh(2\theta)} \oint \tilde{z} T(\tilde{z}) - \frac{c}{24} \left(1 - \frac{1}{\cosh(2\theta)} \right) \right] \\ &= \frac{\pi}{L} \left[\frac{1}{\cosh(2\theta)} \tilde{L}_0 - \frac{c}{24} \left(1 - \frac{1}{\cosh(2\theta)} \right) \right]. \end{aligned} \quad (3.9)$$

Here \tilde{L}_0 the dilatation generator in the \tilde{z} -plane. The action of H_θ in the \tilde{z} -plane is then just a dilatation. Assuming for simplicity $h_\mathcal{O} = \bar{h}_\mathcal{O}$, which will be the relevant case for us here, one has

$$e^{H_\theta t_E} \mathcal{O}(\tilde{z}, \bar{\tilde{z}}) e^{-H_\theta t_E} = \left| \frac{\partial \tilde{z}_{t_E}}{\partial \tilde{z}} \right|^{2h_\mathcal{O}} \mathcal{O}(\tilde{z}_{t_E}, \bar{\tilde{z}}_{t_E}) = \lambda^{2h_\mathcal{O}} \mathcal{O}(\lambda \tilde{z}, \lambda \bar{\tilde{z}}), \quad (3.10)$$

where

$$\tilde{z}_{t_E} = \lambda \tilde{z} \quad \bar{\tilde{z}}_{t_E} = \lambda \bar{\tilde{z}}, \quad (3.11)$$

and with the scaling parameter λ depending on the deformation θ and the Euclidean time t_E

$$\lambda = \exp \frac{\pi t_E}{L \cosh(2\theta)}. \quad (3.12)$$

From here one can go back to the z coordinate using (3.8) on both sides of (3.11)

$$\left(-\frac{z^2 \cosh \theta - \sinh \theta}{z^2 \sinh \theta - \cosh \theta} \right)^{\frac{1}{2}} = \lambda \left(-\frac{z_{t_E}^2 \cosh \theta - \sinh \theta}{z_{t_E}^2 \sinh \theta - \cosh \theta} \right)^{\frac{1}{2}}. \quad (3.13)$$

The map for implementing the time dependence in the UHP is then more conveniently expressed as⁶

$$z_{t_E}^2 = \frac{[(1 - \lambda^2) \cosh(2\theta) - (1 + \lambda^2)] z^2 - (1 - \lambda^2) \sinh(2\theta)}{(1 - \lambda^2) \sinh(2\theta) z^2 - (1 - \lambda^2) \cosh(2\theta) - (1 + \lambda^2)}. \quad (3.14)$$

With a completely similar procedure it is immediate to write the result for the strip

$$w_{t_E} = \frac{L}{2\pi} \log \left[\frac{[(1 - \lambda^2) \cosh(2\theta) - (1 + \lambda^2)] e^{\frac{2\pi}{L} w} - (1 - \lambda^2) \sinh(2\theta)}{(1 - \lambda^2) \sinh(2\theta) e^{\frac{2\pi}{L} w} - (1 - \lambda^2) \cosh(2\theta) - (1 + \lambda^2)} \right], \quad (3.15)$$

⁶As a consistency check, one can take the t_E -derivative on the two sides of equation (3.7), and using the commutation relation between the Virasoro generators and the primary operator, one can match the coefficients mode by mode as in, *e.g.*, [76].

and analogous expressions hold for \bar{z}_{t_E} and \bar{w}_{t_E} .

For later convenience, we write explicitly the form of the transformation in the SSD case, obtained as the $\theta \rightarrow \infty$ limit. The result is conveniently written in terms of t_E as

$$z_{t_E}^2 = \frac{\frac{\pi t_E}{L}(z^2 - 1) + z^2}{\frac{\pi t_E}{L}(z^2 - 1) + 1}, \quad (3.16)$$

or equivalently for the strip

$$w_{t_E} = \frac{L}{2\pi} \log \left[\frac{\frac{\pi t_E}{L}(e^{\frac{2\pi}{L}w} - 1) + e^{\frac{2\pi}{L}w}}{\frac{\pi t_E}{L}(e^{\frac{2\pi}{L}w} - 1) + 1} \right]. \quad (3.17)$$

3.2 Entanglement entropy after the quench

The Euclidean post quench state is described by the density matrix

$$\rho(t_E) = e^{-H_\theta t_E} |\psi_{AB}\rangle \langle \psi_{AB}| e^{H_\theta t_E}. \quad (3.18)$$

The entanglement entropy for the interval $w \in [0, \sigma]$ in this state can be evaluated via the one-point function of a replica twist operator

$$S_\sigma^{(n)} = \frac{1}{1-n} \log \text{Tr} \rho_\sigma^n = \frac{1}{1-n} \log \langle \psi_{AB} | e^{H_\theta t_E} \Phi_n(w = i\sigma, \bar{w} = -i\sigma) e^{-H_\theta t_E} | \psi_{AB} \rangle, \quad (3.19)$$

analytically continuing the result to $n = 1$ as in (2.6).

The evaluation of the time evolved one-point twist correlator in (3.19) can be reduced to the computation in the UHP discussed in section 2. Mapping to the UHP and implementing the time evolution with (3.7) one gets

$$\langle \psi_{AB} | e^{H_\theta t_E} \Phi_n(w, \bar{w}) e^{-H_\theta t_E} | \psi_{AB} \rangle = \left| \frac{\partial z_{t_E}}{\partial w} \right|^{2h_n} \langle \psi_{AB}(\infty) \Phi_n(z_{t_E}, \bar{z}_{t_E}) \psi_{BA}(0) \rangle_{\text{UHP}}. \quad (3.20)$$

This is analogous to (2.8), with the crucial difference that here we are considering a time dependent state. This is reflected in the time dependent insertion point (z_{t_E}, \bar{z}_{t_E}) for the twist field and in the conformal factor, which is now the composition of the map implementing the time dependence with the one relating the strip to the UHP.

Following the approach used in the time independent case, we will approximate $\langle \psi_{AB}(\infty) \Phi_n(z_{t_E}, \bar{z}_{t_E}) \psi_{BA}(0) \rangle_{\text{UHP}}$ with the contribution coming from the identity Virasoro block in the two channels (2.9) and (2.10). After continuing to real time $t_E \rightarrow it$, the correlator will be evaluated as the dominant channel at each time t . The entanglement entropy, is then obtained as the analytic continuation of (3.19) to $n = 1$.

In the next subsection we work out the explicit expression for the correlator (3.20) and its time dependence. We do this first for the simpler SSD case and then for the Möbius evolution. The reader interested in the physical results for the entanglement entropy can move directly to section 3.2.2.

3.2.1 Evaluation of the time dependent correlator

SSD deformation. We consider first the correlator (3.20) approximated by the identity contribution to the A -channel expansion. Reading from (2.17) the UHP result in channel A and analytically continuing to Lorentzian time with $t_E \rightarrow it$, we have

$$\begin{aligned} \langle \psi_{AB} | e^{iH_{\text{SSD}}t} \Phi_n(w, \bar{w}) e^{-iH_{\text{SSD}}t} | \psi_{AB} \rangle \\ \approx C_0^A \alpha^{2h_n} \left(\frac{\partial z_t}{\partial w} \right)^{h_n} \left(\frac{\partial \bar{z}_t}{\partial \bar{w}} \right)^{h_n} (z_t \bar{z}_t)^{(\alpha-1)h_n} (z_t^\alpha - \bar{z}_t^\alpha)^{-2h_n}. \end{aligned} \quad (3.21)$$

Making use of the explicit form of z_t and \bar{z}_t obtained from (3.16) with $z = e^{\frac{i\pi\sigma}{L}}$ and $t_E \rightarrow it$

$$\begin{aligned} z_t &= \frac{L \cos \frac{\pi\sigma}{L} - 2\pi t \sin \frac{\pi\sigma}{L} + iL \sin \frac{\pi\sigma}{L}}{\sqrt{(L \cos \frac{\pi\sigma}{L} - 2\pi t \sin \frac{\pi\sigma}{L})^2 + L^2 \sin^2 \frac{\pi\sigma}{L}}}, \\ \bar{z}_t &= \frac{L \cos \frac{\pi\sigma}{L} + 2\pi t \sin \frac{\pi\sigma}{L} - iL \sin \frac{\pi\sigma}{L}}{\sqrt{(L \cos \frac{\pi\sigma}{L} + 2\pi t \sin \frac{\pi\sigma}{L})^2 - L^2 \sin^2 \frac{\pi\sigma}{L}}}, \end{aligned} \quad (3.22)$$

gives

$$\begin{aligned} \langle \psi_{AB} | e^{iH_{\text{SSD}}t} \Phi_n(w, \bar{w}) e^{-iH_{\text{SSD}}t} | \psi_{AB} \rangle \\ = A_{\Phi_n} \left(\frac{\pi\alpha}{2L} \right)^{2h_n} \left[\left(f(t)^2 + \sin^2 \left(\frac{2\pi\sigma}{L} \right) \right) \sin^2 \left(\frac{\alpha}{2} \delta(t) \right) \right]^{-h_n}, \end{aligned} \quad (3.23)$$

where we used the explicit relation (2.16) between C_0^A and A_Φ .

In the above we have defined the function

$$f(t) \equiv -\frac{2\pi^2 t^2}{L^2} + \left(1 + \frac{2\pi^2 t^2}{L^2} \right) \cos \left(\frac{2\pi\sigma}{L} \right), \quad (3.24)$$

and the phase $\delta(t)$ in (3.23) is defined in terms of the ratio

$$e^{i\delta} \equiv \frac{z_t}{\bar{z}_t}. \quad (3.25)$$

The Lorentzian insertions z_t and \bar{z}_t in (3.22) move on the unit circle defining each a time dependent phase, which difference gives $\delta(t)$. In particular, z_t goes from the initial value $z_{t=0} = e^{\frac{i\pi\sigma}{L}}$ anti-clock-wisely to $e^{i\pi+}$ for $t \rightarrow \infty$. \bar{z}_t goes from $\bar{z}_{t=0} = e^{-\frac{i\pi\sigma}{L}}$ anti-clock-wisely to e^{i0-} . The resulting ratio phase $\delta(t)$ goes from $2\pi\sigma/L$ to π/L

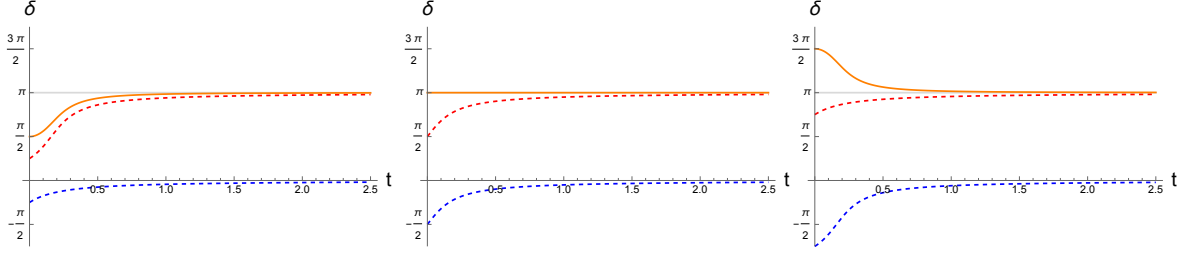


Figure 2: SSD quench. Real time evolution of the phases of z_t in dashed red, \bar{z}_t in dashed blue, and $\delta(t)$ in solid orange. From left to right, $\sigma/L = \frac{1}{4}, \frac{1}{2}, \frac{3}{4}$.

monotonically from below (above) for $\sigma < L/2$ ($\sigma > L/2$). This is illustrated in fig. 2. The result can also be expressed in terms of the function $f(t)$ defined in (3.24) as

$$e^{i\delta} = \frac{f(t) + i \sin\left(\frac{2\pi\sigma}{L}\right)}{\sqrt{f(t)^2 + \sin^2\left(\frac{2\pi\sigma}{L}\right)}}. \quad (3.26)$$

Notice that in the limiting case $\sigma = L/2$ there is actually no time evolution for the phase $\delta(t)$. Despite z_t and \bar{z}_t changing in time, their relative distance along the unit circle remains constant and equal to π . The factor $f(t)^2 + \sin^2\left(\frac{2\pi\sigma}{L}\right)$ in (3.23) has nevertheless a non-trivial evolution, which yields the time dependence for the full correlator.

As discussed in section 2, one can perform a different expansion for the three-point function and approximate the result with the B -channel Virasoro identity block (2.19). The A -channel and B -channel blocks differ by a monodromy, which however does not affect the conformal factor in (3.20). The results for the B -channel follows in a straightforward manner from (2.19) and is obtained performing the replacements $\delta(t) \rightarrow 2\pi - \delta(t)$ and $A_{\Phi_n} \rightarrow B_{\Phi_n}$ in (3.23)

$$\begin{aligned} & \langle \psi_{AB} | e^{iH_{\text{SSD}}t} \Phi(w, \bar{w}) e^{-iH_{\text{SSD}}t} | \psi_{AB} \rangle \\ &= B_{\Phi_n} \left(\frac{\pi\alpha}{2L} \right)^{2h_n} \left[\left(f(t)^2 + \sin^2\left(\frac{2\pi\sigma}{L}\right) \right) \sin^2\left(\frac{\alpha}{2}(2\pi - \delta(t))\right) \right]^{-h_n}. \end{aligned} \quad (3.27)$$

Möbius deformation. For the Möbius case, the evaluation of the correlator (3.20) is performed with a similar computation.

The relevant coordinate transformation implementing the Euclidean evolution is now (3.14). Continuing to Lorentzian time $t_E \rightarrow it$ and defining for compactness the rescaled time variable

$$T \equiv \frac{\pi t}{L \cosh(2\theta)}, \quad (3.28)$$

one obtains

$$z_t = \frac{\cos(T) \cos\left(\frac{\pi\sigma}{L}\right) - e^{2\theta} \sin(T) \sin\left(\frac{\pi\sigma}{L}\right) + i \left(e^{-2\theta} \cos\left(\frac{\pi\sigma}{L}\right) \sin(T) + \cos(T) \sin\left(\frac{\pi\sigma}{L}\right) \right)}{\sqrt{\cos^2(T) - \sin(2T) \sin\left(\frac{2\pi\sigma}{L}\right) \sinh(2\theta) + \sin^2(T) (\cosh(4\theta) - \cos\left(\frac{2\pi\sigma}{L}\right) \sinh(4\theta))}}. \quad (3.29)$$

with the expression for \bar{z}_t obtained via the replacement $\sigma \rightarrow -\sigma$.

The correlator approximated by the identity block contribution in the A -channel can be expressed in the form

$$\begin{aligned} & \langle \psi_{AB} | e^{iH_\theta t} \Phi(w, \bar{w}) e^{-iH_\theta t} | \psi_{AB} \rangle \\ &= A_{\Phi_n} \left(\frac{\pi\alpha}{2L} \right)^{2h_n} \left[\left(f_\theta(T)^2 + \sin^2\left(\frac{2\pi\sigma}{L}\right) \right) \sin^2\left(\frac{\alpha}{2} \delta_\theta(T)\right) \right]^{-h_n}, \end{aligned} \quad (3.30)$$

while the in B -channel it reads

$$\begin{aligned} & \langle \psi_{AB} | e^{iH_\theta t} \Phi(w, \bar{w}) e^{-iH_\theta t} | \psi_{AB} \rangle \\ &= B_{\Phi_n} \left(\frac{\pi\alpha}{2L} \right)^{2h_n} \left[\left(f_\theta(T)^2 + \sin^2\left(\frac{2\pi\sigma}{L}\right) \right) \sin^2\left(\frac{\alpha}{2} (2\pi - \delta_\theta(T))\right) \right]^{-h_n}. \end{aligned} \quad (3.31)$$

The difference with respect to the SSD case completely resides in the explicit form of the function f_θ and phase δ_θ . In particular,

$$f_\theta(T) \equiv -\sin^2(T) \sinh(4\theta) + (\cos^2(T) + \cosh(4\theta) \sin^2(T)) \cos\left(\frac{2\pi\sigma}{L}\right) \quad (3.32)$$

is the finite θ generalization of the function $f(t)$ defined above for the SSD case and recovered as the $\theta \rightarrow \infty$ limit. The phase $\delta_\theta(T)$ is similarly defined as

$$e^{i\delta_\theta} \equiv \frac{z_t}{\bar{z}_t} \quad (3.33)$$

with z_t and \bar{z}_t given in (3.29).

As time evolves, z_t and \bar{z}_t move around the unit circle with T periodicity 2π . Within half a period, z_t goes from the initial value $z_{t=0} = e^{\frac{i\sigma\pi}{L}}$ to $e^{i\pi + \frac{i\sigma\pi}{L}}$, and \bar{z}_t from $\bar{z}_{t=0} = e^{-\frac{i\sigma\pi}{L}}$ to $e^{i\pi - \frac{i\sigma\pi}{L}}$, as portrayed in fig. 3. Despite the individual phases of z_t and \bar{z}_t always increase in time, their difference yields an oscillatory behaviour for $\delta_\theta(T)$ with periodicity π , as shown explicitly in fig. 3. The time evolution of $\delta_\theta(T)$ can be expressed as

$$e^{i\delta_\theta} = \frac{f_\theta(T) + i \sin\left(\frac{2\pi\sigma}{L}\right)}{\sqrt{f_\theta(T)^2 + \sin^2\left(\frac{2\pi\sigma}{L}\right)}}. \quad (3.34)$$

δ_θ starts from the initial value $\frac{2\pi\sigma}{L}$ and reaches an extremal value

$$\delta_{\text{ext}} = \frac{2\pi\sigma}{L} + 2 \arctan\left(\frac{\sin\left(\frac{2\pi\sigma}{L}\right)}{\coth(2\theta) - \cos\left(\frac{2\pi\sigma}{L}\right)}\right) \quad (3.35)$$

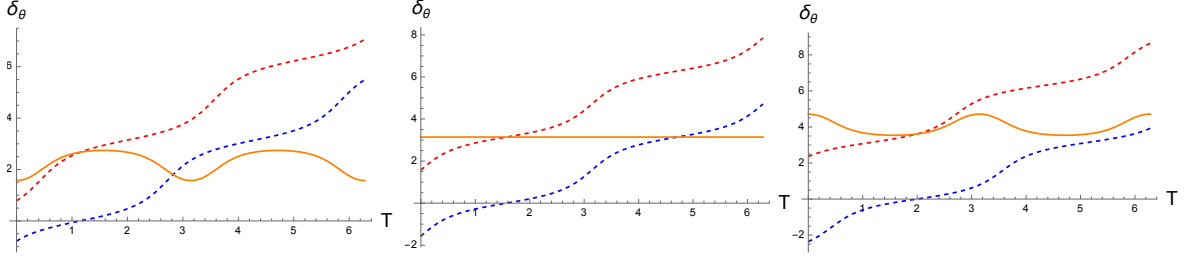


Figure 3: Möbius quench. Real time evolution of the phases of z_t in dashed red, \bar{z}_t in dashed blue, and $\delta(t)$ in solid orange. From left to right, $\sigma/L = \frac{1}{4}, \frac{1}{2}, \frac{3}{4}$. In all plots $\theta = 0.4$.

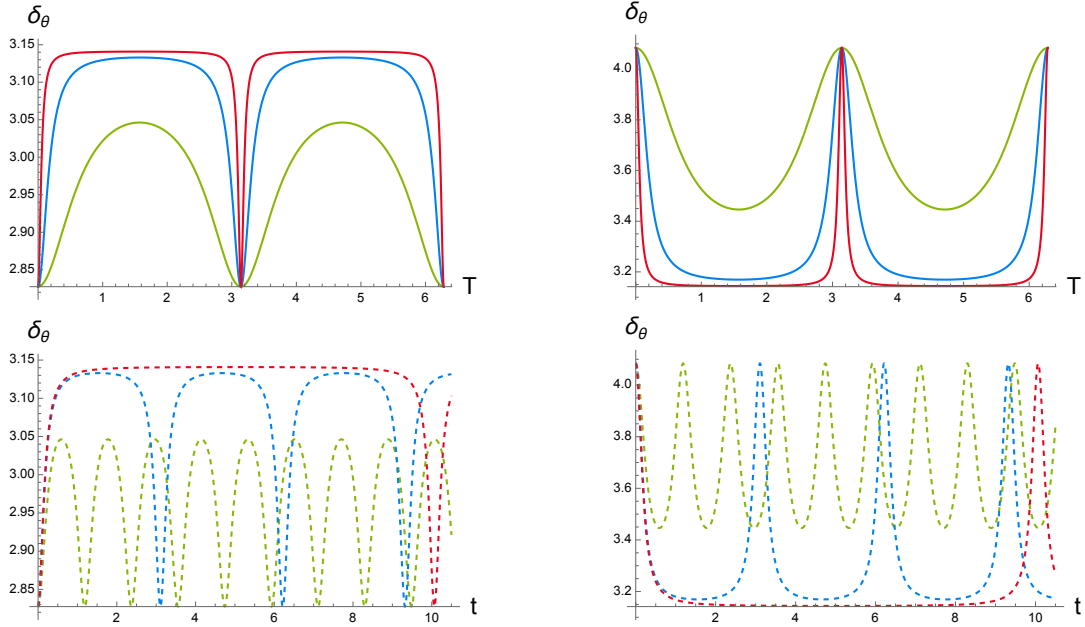


Figure 4: Möbius quench. The oscillatory behaviour for δ_θ is depicted as a function of the effective time T and physical time t , for $\sigma/L = 0.45$ (left) and $\sigma/L = 0.65$ (right). $\theta = 0.3$ (green), 0.9 (blue), 1.5 (red).

for $T = \pi/2$, before going back to the initial value. δ_{ext} represents a maximum for $\sigma < L/2$ and a minimum for $\sigma > L/2$, as visible in fig. 3.

For fixed σ , increasing values of θ give values of δ_{ext} closer to π (see fig. 4). In terms of the physical time t , the oscillatory period increases with θ yielding an effective description where the physical size of the system is rescaled to $L_{\text{eff}} \sim L \cosh(2\theta)$ (see, *e.g.*, [47]). In the $\theta \rightarrow \infty$ limit the effective size goes to infinity, suppressing the return phase, and $\delta_{\text{ext}} \rightarrow \pi$ giving back the SSD evolution in fig. 2.

3.2.2 Evolution of the entanglement entropy

We summarize the result obtained in the previous subsection for the twist one-point function (3.20) in the time dependent state and discuss the ensuing entanglement entropy dynamics. We start considering the SSD case and then move to the Möbius quench.

SSD quench. Under the working assumption that the correlator (3.20) is well approximated by the identity Virasoro block in the A - or B -channel expansion, in Lorentzian time we have

$$\begin{aligned} \langle \psi_{AB} | \Phi_n(w, \bar{w}) | \psi_{AB} \rangle &= \left(\frac{\alpha\pi}{2L} \right)^{2h_n} \left(f(t)^2 + \sin^2 \left(\frac{2\pi\sigma}{L} \right) \right)^{-h_n} \\ &\times \max \left\{ A_{\Phi_n} \left[\sin^2 \left(\frac{\alpha}{2} \delta(t) \right) \right]^{-h_n}; B_{\Phi_n} \left[\sin^2 \left(\frac{\alpha}{2} (2\pi - \delta(t)) \right) \right]^{-h_n} \right\}, \end{aligned} \quad (3.36)$$

with $f(t)$ given in (3.24) and $\delta(t)$ in (3.26).

Plugging (3.36) into the expression for the Rényi entropies (3.19) and continuing to $n = 1$ gives the entanglement entropy for $t > 0$

$$\begin{aligned} S(t) &= \frac{c}{12} \log \left[\left(\frac{2L}{\pi\alpha\epsilon} \right)^2 \left(f^2(t) + \sin^2 \left(\frac{2\pi\sigma}{L} \right) \right) \right] \\ &+ \min \left\{ \frac{c}{12} \log \sin^2 \left(\frac{\alpha}{2} \delta(t) \right) + s_A; \frac{c}{12} \log \sin^2 \left(\frac{\alpha}{2} (2\pi - \delta(t)) \right) + s_B \right\}, \end{aligned} \quad (3.37)$$

where we have reinstated the UV regulator ϵ .

$S(t)$ is thus obtained at each time minimizing over the two competing terms inside the brackets, corresponding to the two channels. Depending on the values of the different parameters, one channel can dominate for all times or there can be a transition from one to the other contribution at some finite time t^* .

Consider first a situation where $s_A = s_B$ and $0 < \alpha < 1$. This is interpreted as the case where the initial state is a high energy eigenstate of the undeformed Hamiltonian on the strip with equal boundary conditions (see section 2.3). In this case, the initial value $\delta(t=0) = 2\pi\sigma/L$ determines which of the two contributions in (3.37) dominates for all times. In fact, the condition to have an exchange of dominance and a transition from the initial channel to the other is to cross the value $\delta(t) = \pi$ at some finite time t^* . However this is only reached asymptotically for $t \rightarrow \infty$ in the SSD case (see fig. 2). The resulting evolution is then qualitatively similar to the case of the ground state with equal boundary conditions on the two sides of the strip, studied in [47].⁷ Indeed

⁷This is recovered for $\alpha = 1$, in which case the two contributions in (3.37) coincide.

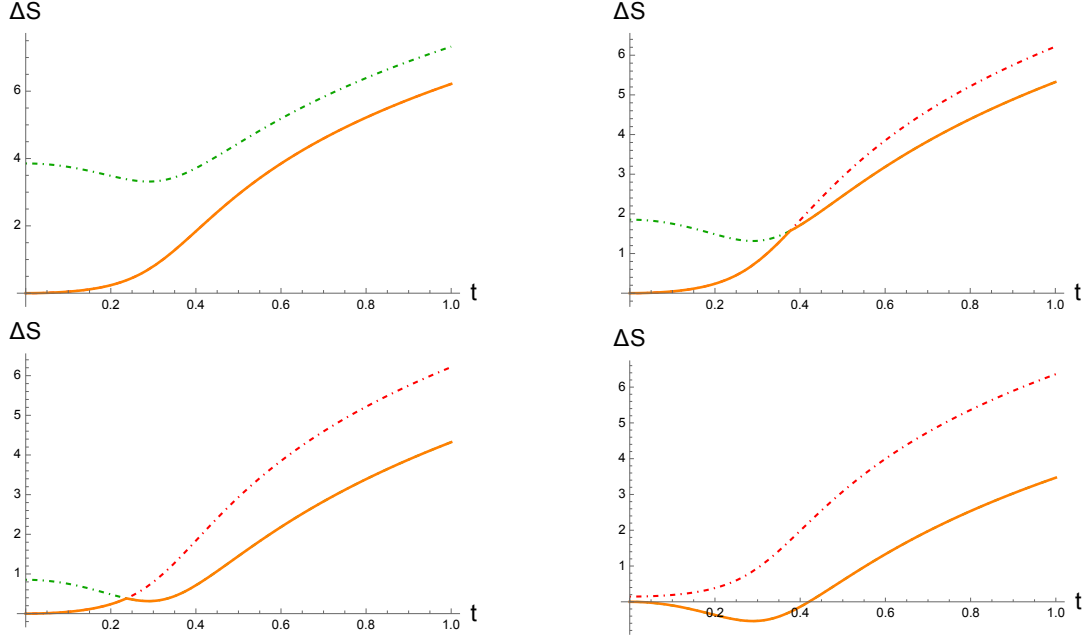


Figure 5: Plot of the entanglement entropy (3.37), rescaled by $12/c$, with the initial value subtracted. The solid line is the entanglement entropy obtained at each time with the minimization procedure over the two competing channels in (3.37). The dot-dashed lines correspond to the two competing channels in their non-dominant phase, red for channel A and green for channel B . The plots show the case of $\sigma/L = 0.15$ and $\alpha = 0.5$, for $\frac{12}{c}(s_B - s_A) = 1, -1, -2, -3$ from top-left to bottom-right.

the late time growth is $S(t) \sim \frac{c}{3} \log t$ and does not exhibit any revival, compatibly with an effective infinite length for the deformed dynamics. It also admits a quasi-particle interpretation, as detailed in [47].

For general values of s_A and s_B , the late time behaviour is unchanged, but at intermediate times the situation is richer and a dynamical exchange of dominance between channel A and B may occur. Figure 5 illustrates an example of how different values of the boundary entropy give different patterns.

In order to have a transition the two contributions in (3.37) should exchange dominance at some time t^* . In other words,

$$\frac{c}{6} \log \frac{\sin\left(\frac{\alpha}{2}\delta(t)\right)}{\sin\left(\frac{\alpha}{2}(2\pi - \delta(t))\right)} = s_B - s_A. \quad (3.38)$$

must have a solution at some value of time t^* . In the SSD case this condition is not satisfied for arbitrary values of s_A and s_B .

The left hand side of (3.38) is always negative and a monotonically increasing function of δ . For $0 < \sigma \leq L/2$, $\delta(t)$ increases monotonically from $2\pi\sigma/L$ at $t = 0$ to

π for $t \rightarrow \infty$. To observe a transition at some finite time t^* , the boundary entropies must then fall within the range

$$\frac{c}{6} \log \frac{\sin\left(\frac{\alpha\pi\sigma}{L}\right)}{\sin\left(\frac{\alpha\pi(L-\sigma)}{L}\right)} < s_B - s_A < 0. \quad (3.39)$$

The monotonicity of $\delta(t)$ also implies that when this condition is satisfied, the initial value of the entropy corresponds to the contribution given by channel A. Therefore the transition will be from channel A to channel B as time increases. On the other hand, when the inequality is violated there is no transition and the dominant channels are

$$\begin{aligned} &A\text{-channel for } s_B - s_A > 0 \\ &B\text{-channel for } s_B - s_A < \frac{c}{6} \log \frac{\sin\left(\frac{\alpha\pi\sigma}{L}\right)}{\sin\left(\frac{\alpha\pi(L-\sigma)}{L}\right)}. \end{aligned} \quad (3.40)$$

Notice that in the limiting case $\sigma = L/2$ the window of values (3.39) for the boundary entropies closes and there is no dynamical transition despite having a time evolving entanglement entropy.

For $L/2 < \sigma < L$ the situation is similar, but $\delta(t)$ now decreases monotonically in time from $2\pi\sigma/L$ to π . In practical terms, the dynamics can be described inverting A and B and a transition from channel B to channel A happens for

$$0 < s_B - s_A < \frac{c}{6} \log \frac{\sin\left(\frac{\alpha\pi\sigma}{L}\right)}{\sin\left(\frac{\alpha\pi(L-\sigma)}{L}\right)}. \quad (3.41)$$

The complementary range of $s_B - s_A$, where there is no transition, can instead be summarized as

$$\begin{aligned} &B\text{-channel for } s_B - s_A < 0 \\ &A\text{-channel for } s_B - s_A > \frac{c}{6} \log \frac{\sin\left(\frac{\alpha\pi\sigma}{L}\right)}{\sin\left(\frac{\alpha\pi(L-\sigma)}{L}\right)}. \end{aligned} \quad (3.42)$$

As shown in fig. 5, for $0 < \sigma \leq L/2$, the transition happens at earlier times for smaller values of $s_B - s_A$. In fact, $\delta(t)$ is a monotonically increasing function of time and solving (3.38) for $\delta(t^*)$ gives the relation

$$\cot\left(\frac{\alpha}{2}\delta(t^*)\right) = \cot(\pi\alpha) + \frac{e^{6(s_B-s_A)/c}}{\sin(\pi\alpha)}, \quad (3.43)$$

On the contrary, for $L/2 < \sigma < L$ the transition happens at larger times for decreasing values of $s_B - s_A$.

Möbius deformation. The Möbius result for the time dependent three point function and the corresponding entanglement entropy can be written in the same form as for the SSD quench

$$\begin{aligned} \langle \psi_{AB} | \Phi_n(w, \bar{w}) | \psi_{AB} \rangle &= \left(\frac{\alpha\pi}{2L} \right)^{2h_n} \left(f_\theta(T)^2 + \sin^2 \left(\frac{2\pi\sigma}{L} \right) \right)^{-h_n} \\ &\times \max \left\{ A_{\Phi_n} \left[\sin^2 \left(\frac{\alpha}{2} \delta_\theta(T) \right) \right]^{-h_n}; B_{\Phi_n} \left[\sin^2 \left(\frac{\alpha}{2} (2\pi - \delta_\theta(T)) \right) \right]^{-h_n} \right\}, \end{aligned} \quad (3.44)$$

and

$$\begin{aligned} S(T) &= \frac{c}{12} \log \left[\left(\frac{2L}{\pi\alpha\epsilon} \right)^2 \left(f_\theta(T)^2 + \sin^2 \left(\frac{2\pi\sigma}{L} \right) \right) \right] \\ &+ \min \left\{ \frac{c}{12} \log \sin^2 \left(\frac{\alpha}{2} \delta_\theta(T) \right) + s_A; \frac{c}{12} \log \sin^2 \left(\frac{\alpha}{2} (2\pi - \delta_\theta(T)) \right) + s_B \right\}. \end{aligned} \quad (3.45)$$

The difference resides in the definition of the function f_θ , in (3.32), and in the time oscillating phase $\delta_\theta(T)$ (see equation (3.34) and discussion around it).

Let us illustrate the case $0 < \sigma \leq L/2$ for simplicity. The physics in the complementary range of σ is easily obtained and substantially amounts to interchanging A and B in the following discussion.

The phase $\delta_\theta(T)$ oscillates with periodicity π between the initial value $2\pi\sigma/L$ and the extremal, maximum, value $\delta_{\text{ext}} < \pi$ in (3.35) (see fig. 4). To have a dynamical phase transition between the two channels in (3.45) the boundary entropies difference must fall within the range

$$\frac{c}{6} \log \frac{\sin \left(\frac{\alpha\pi\sigma}{L} \right)}{\sin \left(\frac{\alpha\pi(L-\sigma)}{L} \right)} < s_B - s_A < \frac{c}{6} \log \frac{\sin \left(\frac{\alpha}{2} \delta_{\text{ext}} \right)}{\sin \left(\frac{\alpha}{2} (2\pi - \delta_{\text{ext}}) \right)} < 0. \quad (3.46)$$

As compared to the SSD case, the range of $s_B - s_A$ which leads to a transition is reduced. Smaller values of the deformation parameter θ correspond to a smaller range of $s_B - s_A$ available for the transition to happen. In the limit $\theta \rightarrow 0$, the transition window in (3.46) closes reflecting the fact that there is no dynamics when the deformation is off.

An example of the entanglement entropy evolution following from the minimization procedure is depicted in fig. 6. The different panels show how depending on the value of $s_B - s_A$ there is or not a transition.

Similarly to the SSD case, outside the range (3.46) there is no transition and the term within brackets in (3.45) is minimized by the

$$\begin{aligned} &A\text{-channel for } s_B - s_A > \frac{c}{6} \log \frac{\sin \left(\frac{\alpha}{2} \delta_{\text{ext}} \right)}{\sin \left(\frac{\alpha}{2} (2\pi - \delta_{\text{ext}}) \right)}, \\ &B\text{-channel for } s_B - s_A < \frac{c}{6} \log \frac{\sin \left(\frac{\alpha\pi\sigma}{L} \right)}{\sin \left(\frac{\alpha\pi(L-\sigma)}{L} \right)}. \end{aligned} \quad (3.47)$$

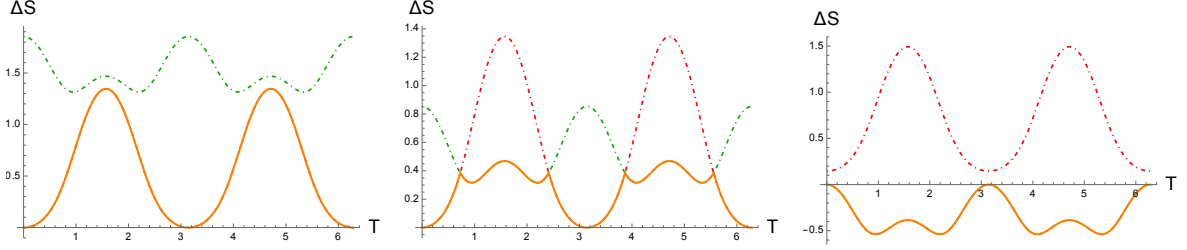


Figure 6: Plot of the entanglement entropy, rescaled by $12/c$, with the initial value subtracted. In all plots $\sigma/L = 0.15, \alpha = 0.5$ and $\theta = 0.3$. From left to right $\frac{12}{c}(s_B - s_A) = -1, -2, -3$. The dot-dashed lines correspond to channel A (red) and B (green) when in their non-dominant phase. The solid line is the entanglement entropy. The dominant channel is A in the left plot and B in the right plot. In the middle there is a transition from channel A to B and back to A happening within each period.

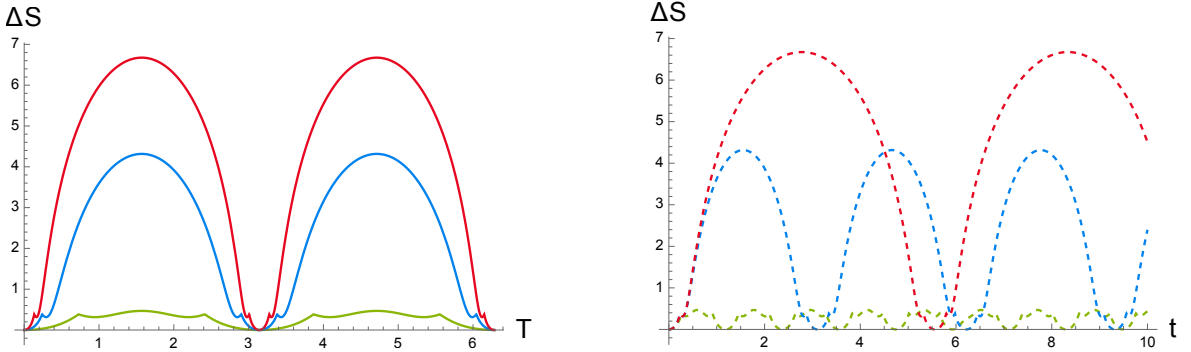


Figure 7: Plot of the entanglement entropy with the initial value subtracted and rescaled by $12/c$. The plots are for $\sigma/L = 0.15, \alpha = 0.5$ and $s_B - s_A = -\frac{c}{6}$. $\theta = 0.3$ (green), 0.9 (blue), 1.5 (red). The plot in terms of the physical time t displays an evolution compatible with an effective spatial size $L_{\text{eff}} \sim L \cosh(2\theta)$.

In fig. 7 we also report sample plots of the time dependence of the entanglement entropy for different values of θ .

One important difference with respect to the SSD quench is the oscillatory character of the dynamics that characterizes the Möbius case. When present, the transition happens at times T^* where

$$\frac{c}{6} \log \frac{\sin\left(\frac{\alpha}{2} \delta_\theta(T^*)\right)}{\sin\left(\frac{\alpha}{2} (2\pi - \delta_\theta(T^*))\right)} = s_B - s_A. \quad (3.48)$$

As seen explicitly in the central panel of fig. 6, when a first transition from channel A to channel B happens at a certain time T^* this will be necessarily followed by a transition back to channel A at a time $\pi - T^*$, and so forth for each period of the

effective time T .

4 Quench with generally deformed Hamiltonians

We have discussed quenches induced by the SSD and Möbius Hamiltonians. On the strip these are constructed through a deformation of the usual CFT Hamiltonian given in terms of level-two Virasoro generators $L_{\pm 2}$.

This construction can be extended to define a general class of deformed Hamiltonians obtained from any subset of the Virasoro generators $\{L_0, L_{\pm k}\}$ with $k \in \mathbb{Z}^+$ (see, *e.g.*, [77–80]), which also form a $sl(2, \mathbb{R})$ algebra [74, 75]. In this section we extend our analysis to this general class of deformed Hamiltonians.

4.1 A general class of deformed Hamiltonians

In analogy with the Möbius Hamiltonian (3.5), the general class of deformed Hamiltonians constructed from $\{L_0, L_{\pm k}\}$ can be written as

$$H_k \equiv H_0 - \frac{\tanh(2\theta)}{2} (H_k^+ + H_k^-) \quad (4.1)$$

where H_0 is the undeformed Hamiltonian (3.3) on an interval of width L , and the deformations H_k^\pm are defined as

$$H_k^\pm = \int_0^L \frac{dw}{2\pi} \left(e^{\pm k\pi w/L} T(w) + e^{\mp k\pi \bar{w}/L} \bar{T}(\bar{w}) \right), \quad (4.2)$$

with $T(w)$ and $\bar{T}(\bar{w})$ defined on the strip.

Mapping the strip to the UHP via $z = e^{\frac{\pi}{L}w}$, we can then write

$$H_k = \frac{\pi}{L \cosh(2\theta)} \oint \left[\cosh(2\theta) z - \frac{\sinh(2\theta)}{2} (z^{-k+1} + z^{k+1}) \right] T(z) - \frac{c\pi}{24L}, \quad (4.3)$$

where the contour integral is in the full complex plane (see appendix A for details).

This makes it explicit that H_k^\pm can be expressed in terms of Virasoro generators in the complex plane, giving

$$H_k^+ + H_k^- = \frac{\pi}{L} \oint (z^{k+1} T(z) + z^{-k+1} T(z)) = \frac{\pi}{L} (L_k + L_{-k}). \quad (4.4)$$

Employing the map

$$\tilde{z}^k = -\frac{z^k \cosh \theta - \sinh \theta}{z^k \sinh \theta - \cosh \theta}, \quad (4.5)$$

allows to bring the total Hamiltonian into the form

$$\begin{aligned} H_k &= \frac{\pi}{L} \left[\frac{1}{\cosh(2\theta)} \oint \tilde{z} T(\tilde{z}) - \frac{c}{24} \left(1 - \frac{k^2 - 1}{\cosh(2\theta)} \right) \right] \\ &= \frac{\pi}{L} \left[\frac{1}{\cosh(2\theta)} \tilde{L}_0 - \frac{c}{24} \left(1 - \frac{k^2 - 1}{\cosh(2\theta)} \right) \right], \end{aligned} \quad (4.6)$$

where \tilde{L}_0 indicates the dilatation generator in the \tilde{z} -coordinate. Therefore, for a primary \mathcal{O}

$$e^{H_k t_E} \mathcal{O}(\tilde{z}, \bar{\tilde{z}}) e^{-H_k t_E} = \lambda^{2h_{\mathcal{O}}} \mathcal{O}(\lambda \tilde{z}, \lambda \bar{\tilde{z}}). \quad (4.7)$$

with

$$\lambda = \exp \frac{\pi t_E}{L \cosh(2\theta)}. \quad (4.8)$$

Mapping back to the UHP, the Euclidean evolution of a CFT primary operator \mathcal{O} under the deformed Hamiltonian can be expressed using (3.7) with the coordinate transformation

$$z_{t_E}^k = \frac{[(1 - \lambda^k) \cosh(2\theta) - (1 + \lambda^k)] z^k - (1 - \lambda^k) \sinh(2\theta)}{(1 - \lambda^k) \sinh(2\theta) z^k - (1 - \lambda^k) \cosh(2\theta) - (1 + \lambda^k)}. \quad (4.9)$$

This can be seen as a $SL(2, \mathbb{R})$ transformation in the k -covering space of the original coordinate z and generalizes the result for the Hamiltonians discussed in the previous section, which is readily recovered for $k = 2$.

4.2 Entanglement entropy after the quench

The time evolution of the entanglement entropy after a quench to the generally deformed Hamiltonian H_k is obtained with the analytic continuation to $n = 1$ of the Rényi calculation (2.5)

$$S_{\sigma}^{(n)} = \frac{1}{1-n} \log \text{Tr} \rho_{\sigma}^n = \frac{1}{1-n} \log \langle \psi_{AB} | e^{H_k t_E} \Phi_n(w = i\sigma, \bar{w} = -i\sigma) e^{-H_k t_E} | \psi_{AB} \rangle. \quad (4.10)$$

Employing z_{t_E} from (4.9) in the evolution equation (3.7), one implements the time dependence as

$$\begin{aligned} &\langle \psi_{AB} | e^{H_k t_E} \Phi_n(w, \bar{w}) e^{-H_k t_E} | \psi_{AB} \rangle \\ &= \left(\frac{\partial z_{t_E}}{\partial w} \right)^{h_n} \left(\frac{\partial \bar{z}_{t_E}}{\partial \bar{w}} \right)^{h_n} \langle \psi_{AB}(\infty) \Phi_n(z_{t_E}, \bar{z}_{t_E}) \psi_{BA}(0) \rangle_{\text{UHP}}. \end{aligned} \quad (4.11)$$

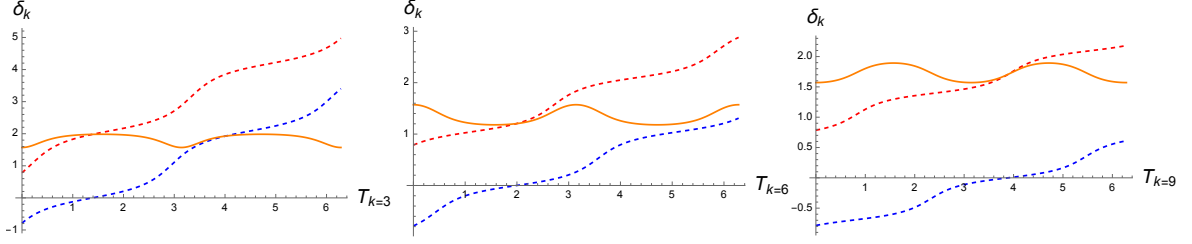


Figure 8: Real time evolution of the phases of z_t dashed red, \bar{z}_t dashed blue, and δ_k . From left to right, $k = 3, 6, 9$. In all plots $\theta = 0.4$, $\sigma/L = \frac{1}{5}$.

4.2.1 Evaluation of the time dependent correlator

Continuing (4.9) to real time $t_E \rightarrow it$ gives

$$z_t^k = \frac{\left(\cos(T_k) \cos\left(\frac{k\pi\sigma}{2L}\right) - e^{2\theta} \sin(T_k) \sin\left(\frac{k\pi\sigma}{2L}\right) + i \left(e^{-2\theta} \cos\left(\frac{k\pi\sigma}{2L}\right) \sin(T_k) + \cos(T_k) \sin\left(\frac{k\pi\sigma}{2L}\right)\right)\right)^2}{\cos^2(T_k) - \sin(2T_k) \sin\left(\frac{k\pi\sigma}{L}\right) \sinh(2\theta) + \sin^2(T_k) (\cosh(4\theta) - \cos\left(\frac{k\pi\sigma}{L}\right) \sinh(4\theta))} \quad (4.12)$$

with \bar{z}_t obtained via the replacement $\sigma \rightarrow -\sigma$. The rescaled time variable T_k is defined as

$$T_k \equiv \frac{k\pi t}{2L \cosh(2\theta)} = \frac{kT_\theta}{2}. \quad (4.13)$$

The Lorentzian insertions z_t and \bar{z}_t start from their respective initial values, $z_{t=0} = e^{i\frac{\pi\sigma}{L}}$ and $\bar{z}_{t=0} = e^{-i\frac{\pi\sigma}{L}}$, and move on the unit circle with phases increasing in time. They go around the circle once over a rescaled T_k period $k\pi$ (see fig. 8).

Using (4.12) and evaluating the UHP correlator in (4.11) as the identity Virasoro block contribution in channel A or B gives

$$\begin{aligned} \langle \psi_{AB} | e^{H_k t_E} \Phi_n(w, \bar{w}) e^{-H_k t_E} | \psi_{AB} \rangle &= \left(\frac{\alpha\pi}{2L}\right)^{2h_n} \left(f_k(T_k)^2 + \sin^2\left(\frac{k\pi\sigma}{L}\right)\right)^{-h_n} \\ &\times \max \left\{ A_{\Phi_n} \left[\sin^2\left(\frac{\alpha}{2} \delta_k(T_k)\right) \right]^{-h_n}; B_{\Phi_n} \left[\sin^2\left(\frac{\alpha}{2} (2\pi - \delta_k(T_k))\right) \right]^{-h_n} \right\}. \end{aligned} \quad (4.14)$$

This is the analogue of (3.36) and (3.44) for the SSD and Möbius cases. In particular, f_k is a generalization of the function f_θ defined in equation (3.32) for the Möbius Hamiltonian⁸

$$f_k(T_k) \equiv -\sin^2(T_k) \sinh(4\theta) + (\cos^2(T_k) + \cosh(4\theta) \sin^2(T_k)) \cos\left(\frac{k\pi\sigma}{L}\right). \quad (4.15)$$

δ_k is the phase difference between z_t and \bar{z}_t , which can be expressed as

$$e^{i\delta_k} \equiv \frac{z_t}{\bar{z}_t} = \left(\frac{(f_k(T_k) + i \sin\left(\frac{k\pi\sigma}{L}\right))^2}{f_k(T_k)^2 + \sin^2\left(\frac{k\pi\sigma}{L}\right)} \right)^{\frac{1}{k}}. \quad (4.16)$$

⁸Notice that f_k also depends on the deformation parameter θ .

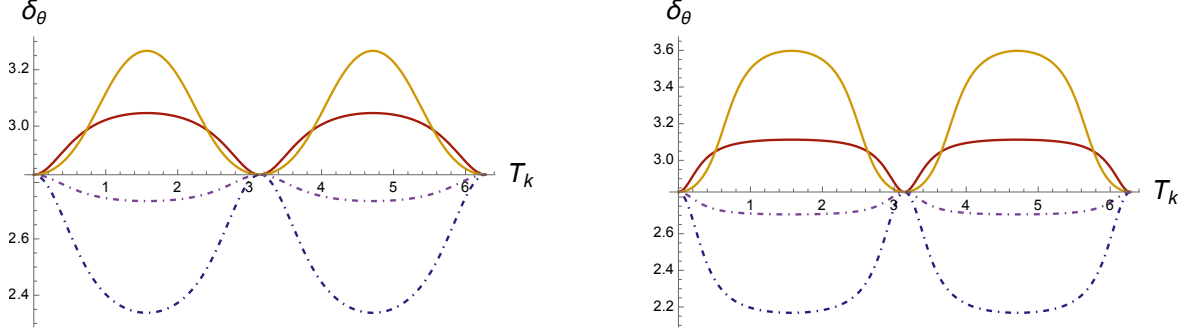


Figure 9: Evolution of the phase δ_k with $\sigma/L = 0.45$. The solid lines are for $k = 2, 5$ going from the bottom-up at $\delta_{k,\text{ext}}$ which is a maximum, *i.e.*, $\frac{2m}{k} < \frac{\sigma}{L} < \frac{2m+1}{k}$. The dashed-dotted lines are for $\delta_{k,\text{ext}}$ corresponding to a minimum, *i.e.*, $\frac{2m+1}{k} < \frac{\sigma}{L} < \frac{2(m+1)}{k}$, with $k = 3, 7$ from the bottom-up. $\theta = 0.3$ on the left and $\theta = 0.6$ on the right, showing how the deformation affects the amplitude of the oscillations.

As displayed in fig. 8, $\delta_k(T_k)$ oscillates with periodicity π between the initial value $\frac{2\pi\sigma}{L}$ and the extremal value

$$\delta_{k,\text{ext}} = \frac{2\pi\sigma}{L} + \frac{4}{k} \arctan \left(\frac{\sin\left(\frac{k\pi\sigma}{L}\right)}{\coth(2\theta) - \cos\left(\frac{k\pi\sigma}{L}\right)} \right). \quad (4.17)$$

$\delta_{k,\text{ext}}$ represents a maximum or a minimum depending on the initial value, *i.e.*, depending on the size σ of the entangling region. For $\sin\left(\frac{k\pi\sigma}{L}\right)$ positive (negative), $\delta_{k,\text{ext}}$ is the maximum (minimum) value reached at half periods of the effective time $T_k = \pi/2, 3\pi/2, \dots$. A few cases for different values of k are illustrated in fig. 9. In the Möbius case ($k = 2$) the initial value was always the minimum (maximum) value for σ smaller (larger) than half of the system (see fig. 4). Here instead the extra parameter k allows for both cases for any value of σ .

We briefly comment on the equivalent of the SSD limit, $\theta \rightarrow \infty$. Also here, in the limit, the returning phase which in the Möbius case distinguished the finite θ deformation from the SSD case disappears. In particular the phase δ_k interpolates monotonically between the initial value and $\delta_{k,\text{ext}}$ in (4.17) in the limit $\theta \rightarrow \infty$. This is attained asymptotically for $t \rightarrow \infty$ and reads

$$\delta_{k,\text{ext}} = 2\pi \frac{(2m+1)}{k} \quad \text{where } m \text{ is such that } \frac{2m}{k} \leq \frac{\sigma}{L} < \frac{2(m+1)}{k}. \quad (4.18)$$

The $k = 2$ case corresponds to the Möbius and SSD case. There $m = 0$ for any σ , giving $\delta_{2,\text{ext}} = \pi$, consistently with the $t \rightarrow \infty$ limit of the phase in the SSD case discussed in section 3.2.

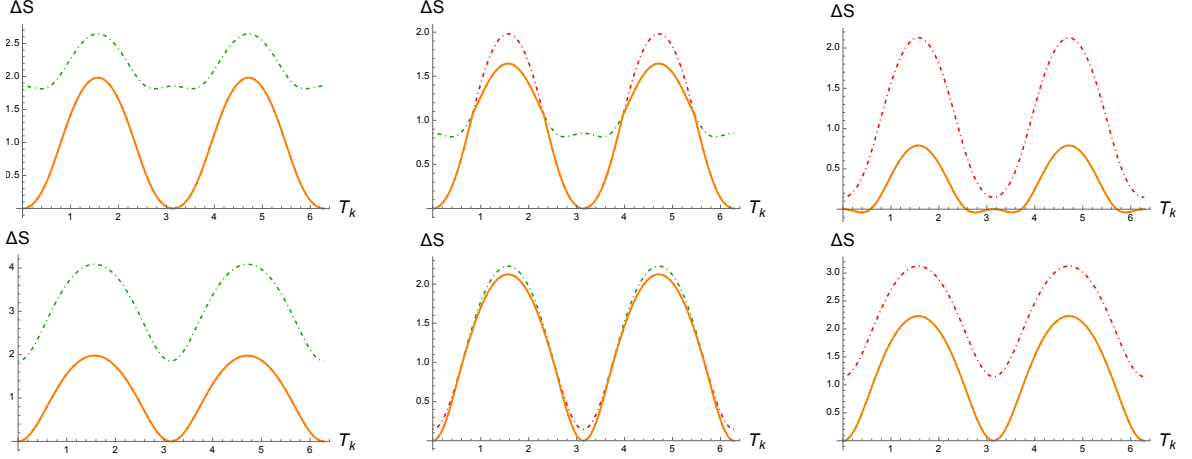


Figure 10: Plot of the entanglement entropy evolution, rescaled by $12/c$ with the initial value subtracted. The solid line is the entanglement entropy obtained from (4.19). The dot-dashed lines correspond to channel A (red) and B (green) when in their non-dominant phase. In all plots $\sigma/L = 0.15$, $\alpha = 0.5$ and $\theta = 0.3$. Top: $k = 3$ and it corresponds to the case $\frac{2m}{k} < \frac{\sigma}{L} < \frac{2m+1}{k}$, with $m = 0$. From left to right $\frac{12}{c}(s_B - s_A) = -1, -2, -3$. Bottom: $k = 8$ and this situation corresponds to the case $\frac{2m+1}{k} < \frac{\sigma}{L} < \frac{2(m+1)}{k}$, with $m = 0$. From left to right $\frac{12}{c}(s_B - s_A) = -2, -3, -4$.

4.2.2 Boundary-induced phase transition

The expression for the entanglement entropy follows in a straightforward manner using the result (4.14) in (4.10) and continuing to $n = 1$

$$S(T) = \frac{c}{12} \log \left[\left(\frac{2L}{\pi\alpha\epsilon} \right)^2 \left(f_k(T_k)^2 + \sin^2 \left(\frac{k\pi\sigma}{L} \right) \right) \right] + \min \left\{ \frac{c}{12} \log \sin^2 \left(\frac{\alpha}{2} \delta_k(T_k) \right) + s_A; \frac{c}{12} \log \sin^2 \left(\frac{\alpha}{2} (2\pi - \delta_k(T_k)) \right) + s_B \right\}. \quad (4.19)$$

$f_k(T_k)$ is defined in equation (4.15) and δ_k oscillates between the initial value $\delta_k(T_k = 0) = 2\pi\sigma/L$ and the extremal value $\delta_{k,\text{ext}}$ in (4.17). Minimizing between the two channels at each instant of time gives the entanglement entropy evolution. Figure 10 illustrate some examples for different choices of the parameters.

Similarly to the Möbius quench, a dynamical transition between the two channels can happen only for specific ranges of the boundary entropies. This condition can be

summarized as

$$\begin{aligned} \frac{c}{6} \log \frac{\sin\left(\frac{\alpha\pi\sigma}{L}\right)}{\sin\left(\frac{\alpha\pi(L-\sigma)}{L}\right)} < s_B - s_A < \frac{c}{6} \log \frac{\sin\left(\frac{\alpha\delta_{k,\text{ext}}}{2}\right)}{\sin\left(\frac{\alpha(2\pi-\delta_{k,\text{ext}})}{2}\right)} \quad \text{for} \quad \frac{2m}{k} < \frac{\sigma}{L} < \frac{2m+1}{k}, \\ \frac{c}{6} \log \frac{\sin\left(\frac{\alpha\delta_{k,\text{ext}}}{2}\right)}{\sin\left(\frac{\alpha(2\pi-\delta_{k,\text{ext}})}{2}\right)} < s_B - s_A < \frac{c}{6} \log \frac{\sin\left(\frac{\alpha\pi\sigma}{L}\right)}{\sin\left(\frac{\alpha\pi(L-\sigma)}{L}\right)} \quad \text{for} \quad \frac{2m+1}{k} < \frac{\sigma}{L} < \frac{2(m+1)}{k} \end{aligned} \quad (4.20)$$

with $m = 0, 1, 2, \dots, [\frac{k}{2} - 1]$, with $[\cdot]$ indicating the integer part.

For a given set of parameters, when $s_B - s_A$ falls in the above range one observes a phase transition between the entanglement evaluated in the two channels at each time T_k^* such that

$$\frac{c}{6} \log \frac{\sin\left(\frac{\alpha}{2}\delta_k(T_k^*)\right)}{\sin\left(\frac{\alpha}{2}(2\pi - \delta_k(T_k^*))\right)} = s_B - s_A. \quad (4.21)$$

The periodic behavior induced by the Möbius type deformation at finite θ implies that the transition happens twice during a period of T_k . One goes from the initial channel to the other at some time T_k^* and then back to the initial channel at $\pi - T_k^*$.

When the difference of boundary entropies is outside the range (4.20), one channel always dominates over the other. More precisely, when $\frac{2m}{k} < \frac{\sigma}{L} < \frac{2m+1}{k}$, the dominant channels are

$$\begin{aligned} \text{A-channel for } s_B - s_A &\geq \frac{c}{6} \log \frac{\sin\left(\frac{\alpha\delta_{k,\text{ext}}}{2}\right)}{\sin\left(\frac{\alpha(2\pi-\delta_{k,\text{ext}})}{2}\right)}, \\ \text{B-channel for } s_B - s_A &\leq \frac{c}{6} \log \frac{\sin\left(\frac{\alpha\pi\sigma}{L}\right)}{\sin\left(\frac{\alpha\pi(L-\sigma)}{L}\right)}. \end{aligned} \quad (4.22)$$

In the complementary range $\frac{2m+1}{k} < \frac{\sigma}{L} < \frac{2(m+1)}{k}$, A and B simply get exchanged

$$\begin{aligned} \text{B-channel for } s_B - s_A &\leq \frac{c}{6} \log \frac{\sin\left(\frac{\alpha\delta_{k,\text{ext}}}{2}\right)}{\sin\left(\frac{\alpha(2\pi-\delta_{k,\text{ext}})}{2}\right)}, \\ \text{A-channel for } s_B - s_A &\geq \frac{c}{6} \log \frac{\sin\left(\frac{\alpha\pi\sigma}{L}\right)}{\sin\left(\frac{\alpha\pi(L-\sigma)}{L}\right)}. \end{aligned} \quad (4.23)$$

5 Holographic dual

In this section we present the gravity dual to the BCFT setup with distinct boundary conditions of section 2.1 and evaluate the holographic entanglement entropy. We then show how to reproduce holographically the result for the time dependent entanglement entropy in the post quench state.

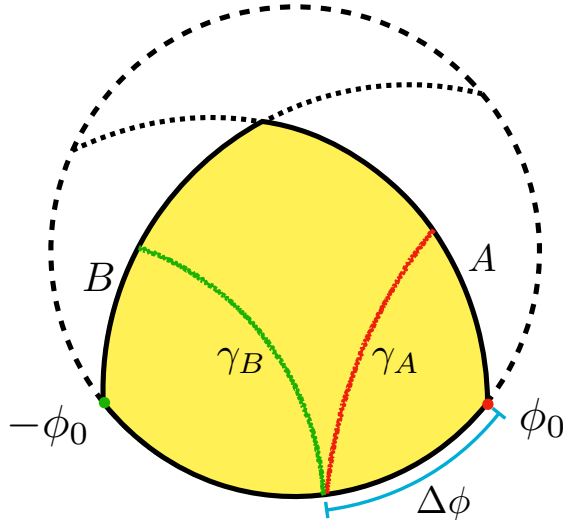


Figure 11: On a given Cauchy slice, the two EOW branes corresponding to the two conformal boundary conditions imposed in the CFT anchor at ϕ_0 and $-\phi_0$ on the asymptotic boundary and intersect in the bulk. The shaded region is the gravitational dual to the CFT we are considering. A defect in the bulk supports the intersection of the two branes. For a given boundary interval $\Delta\phi$ there will be in general two geodesic configurations γ_A and γ_B emanating from the asymptotic boundary and anchoring on the corresponding EOW brane.

Discussions of aspects of the holographic dual of the BCFT setup and related AdS/BCFT constructions appeared in [21–23]. Here we will closely follow the approach of [21], while modifying their construction as to adapt it to a BCFT on an interval at zero temperature.

5.1 Gravitational action and equations of motion

The holographic description of the BCFT setup of section 2.1 involves two end of the world (EOW) branes with different tensions, intersecting at a defect in the bulk of global AdS₃. The branes single out a region of the AdS₃ spacetime which provides the dual geometry for the BCFT on an interval with mixed boundary conditions (see fig. 11).

The total gravitational action of the holographic dual is given by [21]

$$I = I_{\text{EH}} + \sum_{i=A,B} I_{\text{EOW},i} + I_{\text{DEFECT}} + I_{\text{CT}}. \quad (5.1)$$

The first contribution is the Einstein-Hilbert action with negative cosmological constant

Λ plus a Gibbons-Hawking-York term at the AdS boundary ∂AdS

$$I_{\text{EH}} = -\frac{1}{16\pi G_N} \int_{\text{AdS}} \sqrt{-g} (R - 2\Lambda) - \frac{1}{8\pi G_N} \int_{\partial\text{AdS}} \sqrt{-\gamma} K. \quad (5.2)$$

To implement holographically the two distinct boundary conditions of the BCFT, we add in the AdS_3 bulk two EOW branes Σ_i .⁹ The anchoring points on the boundary ∂AdS corresponds to the BCFT interval endpoints. For purely tensional branes, the action is

$$I_{\text{EOW},i} = \frac{1}{8\pi G_N} \int_{\Sigma_i} \sqrt{-h} T_i - \frac{1}{8\pi G_N} \int_{\Sigma_i} \sqrt{-h} K - \frac{1}{8\pi G_N} \int_{\partial\text{AdS} \cap \Sigma_i} \sqrt{-\delta} (\pi - \Theta_i). \quad (5.3)$$

Here $h_{\alpha\beta}$ is the induced metric on the brane and $K_{\alpha\beta}$ its extrinsic curvature. For each brane the equations of motion read

$$K_{\alpha\beta} = (K - T_i) h_{\alpha\beta}. \quad (5.4)$$

This sets the shape of the EOW brane Σ_i in terms of its tension T_i and boundary conditions.

The last term in (5.3) is a Hayward term at the corner $\partial\text{AdS} \cap \Sigma_i$ between the AdS boundary and each brane Σ_i . δ is the induced metric and the internal angle $\Theta_i = \pi$ on shell.

The two branes have in general different tensions T_i and will intersect in the bulk on a worldline Γ . There one needs to include an interaction term in the form of a defect to hold together two distinct branes. The simplest such action is a slight modification of a Hayward term given by

$$I_{\text{DEFECT}} = -\frac{1}{16\pi G_N} \int_{\Gamma} \sqrt{-h_{\Gamma}} (\theta_0 - \hat{\theta}). \quad (5.5)$$

$\theta_0 - \pi$ can be regarded as the effective tension of the defect and $\hat{\theta}$ is the internal angle at the branes intersection. On shell this is related to the defect tension via the condition

$$\hat{\theta} = \theta_0. \quad (5.6)$$

Finally, the action includes appropriate counterterms I_{CT} to renormalize the divergences coming from near the AdS boundary [21].

⁹While strictly speaking these objects are strings in AdS_3 , we will use the nomenclature that is most common in this literature and refer to them as branes, as in the higher dimensional settings.

5.2 Intersecting branes in AdS_3

We first briefly review the AdS dual to a BCFT on an interval with equal boundary conditions at the endpoints.

Consider empty AdS_3 with metric

$$ds^2 = -\frac{r^2 + 1}{R^2} dt^2 + \frac{dr^2}{r^2 + 1} + r^2 d\phi^2, \quad (5.7)$$

with $r \in [0, \infty)$, $t \in (-\infty, \infty)$ and $\phi \in [-\pi, \pi]$. The AdS radius is set to one and R denotes the radius of the boundary circle.

Take a purely tensional brane of tension T emanating from a point $0 \leq \phi_0 < \pi$ on ∂AdS_3 . On shell, the brane has the following static profile

$$r = \frac{k}{\sin(\phi - \phi_0)}, \quad (5.8)$$

where we have defined the combination

$$-\infty < k \equiv \frac{T}{\sqrt{1 - T^2}} < \infty. \quad (5.9)$$

The brane connects antipodal points on ∂AdS_3 . If $k < 0$ the brane spans in the bulk the angular interval $-\pi + \phi_0 \leq \phi \leq \phi_0$ while for $k > 0$ it spans the interval $\phi_0 \leq \phi \leq \pi \cup -\pi \leq \phi \leq -\pi + \phi_0$. Retaining the AdS bulk geometry comprised between the brane and the portion of boundary with angular range $-\pi + \phi_0 \leq \phi \leq \phi_0$ gives the dual for the BCFT on the strip with equal boundary conditions (see for example [16, 17]).

To implement two distinct boundary conditions as in section 2.1, we consider two static branes anchored at symmetric points about $\phi = 0$, *i.e.*, at $\pm\phi_0$ with $0 < \phi_0 < \frac{\pi}{2}$. In the intersecting configuration, we retain the AdS bulk portion that has angular boundary range $-\phi_0 \leq \phi \leq \phi_0$, as illustrated in fig. 11.¹⁰

We parametrize the two branes profiles as

$$r = \frac{k_A}{\sin(\phi - \phi_0)} \quad \text{and} \quad r = -\frac{k_B}{\sin(\phi + \phi_0)}, \quad (5.10)$$

without making any assumption about the signs and values of the tension parameters. With this choice, for equal tensions $k_A = k_B$ and $\phi_0 = \pi/2$ the two branes coincide. Notice that for $k_A > 0$ ($k_A < 0$) the first brane spans the angular coordinate range $\phi_0 \leq \phi \leq \pi \cup -\pi \leq \phi \leq -\pi + \phi_0$ ($-\pi + \phi_0 \leq \phi \leq \phi_0$). If $k_B > 0$ ($k_B < 0$) the

¹⁰One could in principle also consider the complementary range $-\pi \leq \phi \leq -\phi_0 \cup \phi_0 \leq \phi \leq \pi$ or, equivalently, $\frac{\pi}{2} < \phi_0 < \pi$ [21].

second brane spans the angular coordinate range $-\pi \leq \phi \leq -\phi_0 \cup -\phi_0 + \pi \leq \phi \leq \pi$ ($-\phi_0 \leq \phi \leq -\phi_0 + \pi$) (see fig. 11).

On any fixed time slice, the branes intersect at a point (r_*, ϕ_*) such that

$$r_*^2 = \frac{k_A^2 + k_B^2 + 2k_A k_B \cos 2\phi_0}{\sin^2 2\phi_0} \quad (5.11)$$

$$\tan \phi_* = \frac{k_B - k_A}{k_A + k_B} \tan \phi_0. \quad (5.12)$$

In particular we have

$$\phi_* \in \begin{cases} [\phi_0, \pi - \phi_0] & \text{if } k_A > 0, k_B < 0 \\ [\pi - \phi_0, \pi] \cup [-\pi, -\pi + \phi_0] & \text{if } k_A > 0, k_B > 0 \\ [-\phi_0, \phi_0] & \text{if } k_A < 0, k_B < 0 \\ [-\pi + \phi_0, -\phi_0] & \text{if } k_A < 0, k_B > 0 \end{cases}. \quad (5.13)$$

Also, notice that in the limit $\phi_0 \rightarrow \pi/2$, the radial coordinate r_* of the branes intersection goes to infinity, but this limiting value can be approached for any choice of T_A and T_B .

The angle $\hat{\theta}$ between the branes at the intersection point is obtained in terms of the unit normals n_A, n_B . Defining them to be outward-pointing with respect to the bulk region between the branes gives

$$\begin{aligned} n_{A\mu} &= \pm \sqrt{\frac{\sin^2(\phi - \phi_0)}{1 + k_A^2}} \left(0, 1, \frac{k_A}{\sin(\phi - \phi_0) \tan(\phi - \phi_0)} \right), \\ n_{B\mu} &= \pm \sqrt{\frac{\sin^2(\phi + \phi_0)}{1 + k_B^2}} \left(0, 1, -\frac{k_B}{\sin(\phi + \phi_0) \tan(\phi + \phi_0)} \right), \end{aligned} \quad (5.14)$$

with the \pm sign respectively for positive and negative values of the tension parameters. Keeping track of the sign of the tensions and using equation (5.10), (5.11) and (5.12), one obtains the relation

$$\cos(\pi - \hat{\theta}) = n_{A\mu} n_{B\nu} g^{\mu\nu} = \frac{k_A k_B - \cos 2\phi_0}{\sqrt{(1 + k_A^2)(1 + k_B^2)}} \quad (5.15)$$

for any sign of k_A and k_B .

On shell, the brane intersection angle coincides with the tension parameter of the defect sustaining the intersection, $\theta_0 = \hat{\theta}$, which is then related to the opening angle ϕ_0 as

$$\cos 2\phi_0 = k_A k_B + \sqrt{(1 + k_A^2)(1 + k_B^2)} \cos \theta_0. \quad (5.16)$$

The case in which the branes have the same tension and there is no intersection nor defect, $\theta_0 = \pi$, yields $\phi_0 = \pi/2$ consistently with the parametrization (5.10).

5.2.1 Matching the BCFT setup

We now match the BCFT parameters of the setup in section 2.1 to the holographic ones. The length L of the CFT interval is given by the opening between the two branes at the AdS boundary

$$L = 2\phi_0 R. \quad (5.17)$$

The conformal dimension h_ψ of the BCC operator is directly related to the opening angle ϕ_0 . The relation is obtained remembering that h_ψ is determined by the gap in energy between the state with and without BCC operator, *i.e.*, between the state with mixed boundary conditions and the ground state with homogeneous boundary conditions (see equation (2.3)). Holographically this is the energy difference between the configuration with two intersecting branes and the one with a single brane.¹¹ Evaluating the corresponding bulk actions, the shift in energy is found to be [21]

$$h_\psi = \frac{L \Delta E}{\pi} = \frac{c}{24} \left(1 - \frac{4\phi_0^2}{\pi^2} \right) \quad (5.18)$$

giving

$$\frac{2\phi_0}{\pi} = \sqrt{1 - \frac{24h_\psi}{c}}. \quad (5.19)$$

Notice that $h_\psi \propto c$ and the spectrum goes from arbitrarily close to 0 to $c/24$ [21, 22]. Therefore, in the holographic realization there exists a BCC operator implementing the change in boundary conditions with an arbitrary small change in energy. That is, for any set of mixed boundary conditions holographically specified by T_A and T_B , the lowest energy state has at leading order in c the same energy of a the ground state with homogeneous boundary conditions.

5.3 Holographic entanglement entropy

To reproduce holographically the entanglement entropy result for the strip with different boundary conditions, equation (2.22), we shall evaluate the Ryu-Takayanagi [57] formula

$$S = \frac{\text{Area } \gamma}{4G_N} \quad (5.20)$$

in the static geometry with EOW branes [16, 17]. In AdS_3 , the surfaces γ are regulated geodesics and the area term is evaluated as the geodesic proper length, $\text{Area } \gamma = d_\gamma$.

In our setup we need to consider the minimal length geodesic extending from a point on the boundary to the EOW branes. There are in general two competing,

¹¹This is actually independent from the tension of the brane, *e.g.*, [81].

locally extremal, curves one should take into account. The minimal length geodesic extending into the bulk and ending on the brane with tension parameter k_A and the one ending on the brane with tension k_B , see fig. 11.

5.3.1 Geodesic computation

Let us start reviewing the case of a geodesic stretching between a boundary point and a single brane in AdS_3 . The proper length d_γ of a constant time geodesic γ in AdS_3 between two generic points is given by

$$\cosh d_\gamma = \sqrt{(r_1^2 + 1)(r_2^2 + 1)} - r_1 r_2 \cos(\phi_1 - \phi_2) . \quad (5.21)$$

We take one extrema to be at a generic point (r_b, ϕ_b) on the EOW brane with profile

$$r_b = \frac{k}{\sin \phi_b} . \quad (5.22)$$

The other is taken on the regulated AdS boundary at r_∞ displaced by $\tilde{\phi}$ from the brane anchoring point at $\phi = 0$, that is at $(r_\infty, \tilde{\phi})$. For the length d_γ this gives

$$\cosh d_\gamma \approx r_\infty \left(\sqrt{\frac{k^2}{\sin^2 \phi_b} + 1} - \frac{k}{\sin \phi_b} \cos(\tilde{\phi} - \phi_b) \right) , \quad (5.23)$$

where we made a large r_∞ expansion and used (5.22) to express r_b in terms of ϕ_b .

Extremizing the length over the possible ending points on the brane sets¹²

$$\sin \phi_{b,\text{ext}} = \frac{k \sin |\tilde{\phi}|}{\sqrt{k^2 + \cos^2 \tilde{\phi}}} \quad (5.24)$$

and selects the geodesic with minimal length amongst all geodesics ending on the brane. This has length

$$d_\gamma = \log \left[2r_\infty \left(-k \sin \tilde{\phi} + \sqrt{1 + k^2} \sin |\tilde{\phi}| \right) \right] . \quad (5.25)$$

The single brane analysis is immediately extended to the situation with two intersecting EOW branes as in equation (5.10). We parametrize the boundary point from where the geodesic emanates in terms of the distance $0 < \Delta\phi < 2\phi_0$ from brane A . The point is then at the angular location $\phi_0 - \Delta\phi$.

There are now two locally minimal geodesics to consider. One is the geodesic γ_A ending on the EOW brane A , which has length

$$d_{\gamma_A} = \log [2r_\infty \sin \Delta\phi] + \text{arcsinh } k_A . \quad (5.26)$$

¹²Notice that for $\pi/2 < |\tilde{\phi}| < \pi$ this means that $\pi/2 < |\phi_b| < \pi$.

The other geodesic γ_B is the minimal length one between those ending on the brane B . This has length

$$d_{\gamma_B} = \log [2r_\infty \sin(2\phi_0 - \Delta\phi)] + \operatorname{arcsinh} k_B. \quad (5.27)$$

Notice that this is obtained from (5.25) taking into account that the equation giving the brane profile B in (5.10) has an overall extra minus sign as compared to (5.22).

For any given boundary interval $\Delta\phi$, the geodesic which has minimal length between (5.26) and (5.27) is the one selected by the Ryu-Takayanagi formula (5.20)

$$S = \frac{\min\{d_{\gamma_A}, d_{\gamma_B}\}}{4G_N}. \quad (5.28)$$

As a function of $\Delta\phi$, a dominance transition from one geodesic to the other happens for a value $\Delta\phi_t$ corresponding to $d_{\gamma_A} = d_{\gamma_B}$. Namely

$$\cot \Delta\phi_t = \csc 2\phi_0 \frac{k_A + \sqrt{1 + k_A^2}}{k_B + \sqrt{1 + k_B^2}} + \cot 2\phi_0, \quad (5.29)$$

which is consistently within the range $0 < \Delta\phi_t < 2\phi_0$.

Notice that the two geodesics may not always exist at the same time in our setup. For instance, γ_A may cease to exist for a large enough $\Delta\phi > \Delta\phi_A$. The limiting value corresponds to the situation where the endpoint of γ_A on the brane $\phi_{b,\text{ext}}$ coincides with the branes intersection point ϕ_* . That is, when

$$\sin(\phi_* - \phi_0) = \frac{k_A \sin \Delta\phi_A}{\sqrt{k_A^2 + \cos^2 \Delta\phi_A}}. \quad (5.30)$$

Substituting the explicit expression (5.12) for ϕ_* gives¹³

$$\cot \Delta\phi_A = -\frac{\csc 2\phi_0 (k_A \cos 2\phi_0 + k_B)}{\sqrt{k_A^2 + 1}}. \quad (5.31)$$

Similarly γ_B may not exist for a small enough value of $\Delta\phi < \Delta\phi_B$. Here $\Delta\phi_B$ is given by

$$\cot(2\phi_0 - \Delta\phi_B) = -\frac{\csc 2\phi_0 (k_B \cos(2\phi_0) + k_A)}{\sqrt{k_B^2 + 1}}. \quad (5.32)$$

However, one can check explicitly that

$$\Delta\phi_B < \Delta\phi_t < \Delta\phi_A, \quad (5.33)$$

so that at the transition point both geodesic configurations do actually exist in our setup.

¹³This can formally give a value of $\Delta\phi_A$ outside the physical range $0 < \Delta\phi < 2\phi_0$. In such a case γ_A always exists in the setup we are looking at. A similar consideration applies to $\Delta\phi_B$.

5.3.2 Matching the BCFT computation

To show that the holographic entanglement entropy in (5.28) matches the static result in section 2.3, we need to express it in terms of the dual CFT parameters. For the BCFT cutoff ϵ and size of the entangling interval σ , we have the relations

$$\frac{r_\infty}{R} = \frac{1}{\epsilon} \quad R\Delta\phi = \sigma. \quad (5.34)$$

These directly follow from matching the conformal boundary of AdS metric (5.7) with the BCFT geometry. Expressing everything in terms of the physical size L through (5.17) and using the relation (5.19) yields

$$r_\infty = \frac{L}{\alpha\pi\epsilon} \quad \Delta\phi = \frac{\sigma L}{\alpha\pi}, \quad (5.35)$$

where we have used $\alpha = \sqrt{1 - 24h_\psi/c}$ (see equation (2.14)).

Substituting these into the expressions for the geodesics length (5.26) and (5.27) and using the relation $c = 3/2G_N$, we get from (5.28)

$$S = \frac{c}{6} \log \frac{2L}{\pi\alpha\epsilon} + \min \left\{ \frac{c}{6} \log \sin \frac{\alpha\pi\sigma}{L} + \frac{c}{6} \operatorname{arcsinh} k_A; \frac{c}{6} \log \sin \frac{\alpha\pi(L-\sigma)}{L} + \frac{c}{6} \operatorname{arcsinh} k_B \right\}, \quad (5.36)$$

By matching the brane A, B with the conformal boundary condition A, B in the CFT via the identification [16, 17]

$$s_{A,B} = \frac{c}{6} \operatorname{arcsinh} k_{A,B}, \quad (5.37)$$

one exactly reproduces the result (2.22) for the static case derived in section 2.3.

The holographic computation of the entanglement entropy in the post quench state involves considering geodesics in a AdS_3 time dependent geometry [16, 17, 57, 58]. In principle it should be possible to work explicitly the form of this dual geometry, which one expects to be constructed from two EOW branes with a non-trivial time dependent profile.¹⁴ Here we will simply show how to reproduce the time dependent entanglement entropy.

The static state yielding the above result and the time dependent post quench state are related on the CFT side by a transformation of the conformal coordinates. This map can be extended to a diffeomorphism in AdS_3 that relates the geometries

¹⁴See [36, 37, 82] for this type of analysis performed in the case of a CFT on a circle.

dual to the CFT states described in the two sets of coordinates [83, 84].¹⁵ The length of geodesics relevant for the post quench state can then be obtained using this local equivalence of AdS₃ geometries (see, *e.g.*, [52, 87, 88]).

Let us start expressing the static result (5.36) using coordinates that match those defined on the strip in section 2. For this we can simply focus on the asymptotic form of the AdS₃ metric (5.7), which we can write in Euclidean as

$$ds^2 \approx \frac{dr^2}{r^2} + \frac{r^2}{R^2}(d\tau^2 + R^2 d\phi^2) = \frac{dw d\bar{w} + du^2}{u^2}. \quad (5.38)$$

We made the identifications

$$u = \frac{R}{r} \quad w = \tau + iR\phi \quad \bar{w} = \tau - iR\phi. \quad (5.39)$$

and (w, \bar{w}) match the Euclidean coordinates on the strip.

The entanglement entropy result obtained from the static geometry analysis is then rewritten as

$$S = \min \left\{ \frac{c}{6} \log \frac{2L}{\pi \alpha u_\infty} \sin \frac{\alpha \pi |w_\infty - \bar{w}_\infty|}{2L} + s_A; \frac{c}{6} \log \frac{2L}{\pi \alpha u_\infty} \sin \frac{\alpha \pi (2L - |w_\infty - \bar{w}_\infty|)}{2L} + s_B \right\} \quad (5.40)$$

and using the identifications

$$\begin{aligned} w_\infty &= i\sigma \\ \bar{w}_\infty &= -i\sigma \\ u_\infty &= \epsilon \end{aligned} \quad (5.41)$$

reproduces the result (5.36).

The holographic entanglement entropy for the time dependent state is instead obtained with a different identification

$$\begin{aligned} w_\infty &= w_{t_E}(w = i\sigma) \\ \bar{w}_\infty &= \bar{w}_{t_E}(\bar{w} = -i\sigma) \\ u_\infty &= \epsilon \sqrt{w'_{t_E}(w = i\sigma) \bar{w}'_{t_E}(\bar{w} = -i\sigma)}. \end{aligned} \quad (5.42)$$

This is the asymptotic form of the bulk diffeomorphism corresponding to the CFT map relating the initial state to the post quench state [83, 84]. It pulls back the point $w_\infty, \bar{w}_\infty, u_\infty$ in the time independent geometry to the point σ and bulk cutoff ϵ in the

¹⁵A subtlety is that the time governing the evolution t_E appears as a parameter in the map and not as a component of the complex CFT coordinates. The map relates for each t_E the initial state static geometry to an auxiliary geometry with its own time slicing where the geodesic length giving the time dependent result can be computed. See, *e.g.*, [85, 86] for related discussions.

geometry dual to the time dependent state at time t_E . This can be thought of as the bulk counterpart of the fact that on the CFT side an operator in the time dependent state at a given time t_E can be expressed in terms of the initial static state operator through the map w_{t_E} .

Using the identification (5.42) in (5.40), and continuing to Lorentzian time $t_E \rightarrow it$, it is quite immediate to see how this reproduces the post quench result. To illustrate this more explicitly we consider the example of the SSD quench, other cases follow with similar computations. Using in (5.42) the explicit form of the SSD time dependent map (3.17) and continuing to Lorentzian time $t_E \rightarrow it$, one can easily check that

$$u_\infty = \epsilon \sqrt{w'_t(w = i\sigma) \bar{w}'_t(\bar{w} = -i\sigma)} = \epsilon \sqrt{\frac{1}{f(t)^2 + \sin^2\left(\frac{2\pi\sigma}{L}\right)}} \quad (5.43)$$

which matches the time dependent factor accompanying the cutoff in the expressions for the SSD entanglement entropy (3.37). Similarly, in the argument of the sin in the holographic formula (5.40) one recognizes $\delta(t)$, the phase defined in (3.37)

$$|\omega_t - \bar{\omega}_t| = \frac{L}{\pi} \left| \log \frac{z_t}{\bar{z}_t} \right| = \frac{L}{\pi} \delta(t). \quad (5.44)$$

To be explicit we used the relation between the CFT coordinates on the strip and in the UHP to write the middle expression.

6 Discussion

We studied the role of boundary effects for the entanglement entropy in a CFT defined on an interval with mixed boundary conditions after an inhomogeneous quench. We considered a quench protocol where the initial state is an eigenstate of L_0 and the evolution is driven by a deformation of the standard CFT Hamiltonian. In particular, we analyzed the case of the SSD and Möbius deformation, as well as a general class of Hamiltonian deformations defined in terms of $sl(2, \mathbb{R})$ subalgebras of the full Virasoro algebra. We probed the entanglement dynamics in terms of the entanglement entropy for a portion of the system that includes one of the boundaries.

Although the setup and the techniques employed are in large part general, our analysis focused on the case of holographic CFTs. In this context it is natural to focus on the universal contribution to the entanglement entropy coming from the identity Virasoro block. This is expected to give the leading contribution at large c and to capture the physics of semiclassical gravity in the holographic AdS_3 dual.

Our analysis reveals an entanglement dynamics with a characteristic phase transition pattern governed by boundary effects. The mixed conformal boundary conditions,

A and B , in our setup give rise to two competing phases for the entanglement entropy obtained from the conformal family of the stress tensor, as described in section 2.3. For the initial static state, one or the other phase dominates depending on the size of the entangling region and the relative value of the boundary entropies. The post-quench evolution, on the other hand, turns out to allow for a dynamical transition between these phases. For a fixed entangling region, the transition pattern is determined by the relative amount of degrees of freedom associated with the two conformal boundaries, as encoded in the boundary entropies $s_{A,B}$. When the number of degrees of freedom encoded in s_A and s_B are close enough to each other, in a sense made quantitative in section 3.2 and 4.2.2, the quench dynamics induces a transition from the initial phase to the other. For boundary entropies values that differ significantly, the initial phase instead dominates for all time. This is a common feature of all the deformations we considered in this work, but the details depend on the specific deformation considered. In particular the precise range of $s_B - s_A$ for which the transition occur depends on the deformation.

At the kinematic level the entanglement dynamics of each phase is analogous to the case of homogeneous boundary conditions [47]. For the Möbius and generalized $sl(2, \mathbb{R})$ deformations the entanglement entropy exhibits a kinematics compatible with a finite size system, characterized by an effective length which details are determined by the deformation parameters. This implies also a recurrent behaviour for the phase transition pattern. Within one period the phases alternate, going from, *e.g.*, phase A to B , and back to the initial phase A , as depicted in fig. 7 and 10. In the SSD case the kinematic is compatible with the one of an infinite dimensional system, with no return phase and a $\sim \log t$ growth of the entanglement entropy at lates times. Still, the presence of a phase transition signals the finiteness of the system with different conformal boundary conditions.

As we discussed in section 5, our CFT analysis finds a direct match on the geometric AdS_3 description. The holographic dual of the boundary CFT setup involves two EOW branes anchored on the boundary and extending in the AdS_3 bulk, where they intersect. This construction selects a portion of the AdS_3 geometry comprised between the AdS_3 boundary and the two intersecting branes. In this setup the brane tensions T_A and T_B are in one to one correspondence with the conformal boundary conditions A and B and determine the value of the boundary entropies. The two CFT channels described in section 2.3 have a direct correspondence in the two competing Ryu-Takayanagi surfaces one can draw in the asymptotically AdS_3 geometry. These are given by geodesics extending from the boundary of AdS to the EOW branes, as depicted in fig. 11.

In section 5.3, we showed explicitly how the holographic entanglement entropy exactly matches the CFT result. We obtained this result exploiting directly the local equivalence of asymptotically AdS_3 geometries and the dictionary relating CFT maps to bulk diffeomorphisms. We did not analyze explicitly the details of the time dependent geometries dual to the post quench state for the various deformations. It should be possible to do so along the lines of [36–38] which studied the case of a CFT on a circle.

Double holography and quantum extremal surface

Our analysis lends itself for an interpretation in the context of double holography. In fact, there is a third complementary description which is available for our system, the so called brane perspective, as we schematically discuss in the following.

There, the bulk spacetime enclosed between the asymptotic AdS boundary and the EOW branes is integrated out leaving behind an effective gravitational theory on each brane [89–91]. In the case of intersecting branes with a defect supporting the intersection, we have two gravitational spacetimes, given by portions of AdS_2 with different effective cosmological constants. These are separated from one another by the defect on one side and in contact with the same non-gravitational CFT region on the other side.

Our entanglement entropy result can be interpreted in this perspective as a generalized entropy computation [11–15, 92]. In the BCFT perspective, the region we considered includes the boundary with conformally invariant boundary condition A . In the brane description, this corresponds to considering the entanglement entropy for the interval $[0, \sigma]$ in the 2d CFT and an adjacent portion of the gravitational space. Which portion of the AdS_2 exactly enters is determined by the generalized entropy formula itself, which requires finding the quantum extremal surface (QES) [92]. In double holography the location of the latter corresponds to the intersection of the Ryu-Takayanagi surface with the brane (see, *e.g.*, [13, 93–96]). The region enclosed by the QES in the brane perspective then goes from σ to this point, as depicted in fig. 12.

In the simplest case of a SSD quench, one can interpret the dynamical phase transition as follows:¹⁶ at the initial time of the post quench evolution the QES is inside universe A . As time evolves this goes deeper into the AdS_2 bulk of universe A . At the phase transition time, the QES surface jumps to universe B selecting a region that extends from σ all the way to cover the entire universe A , the bulk defect and part of

¹⁶Here we are thinking in a quasi-static manner. A complete picture would require knowing the exact time dependent post quench geometry and the time dependent profile of the branes

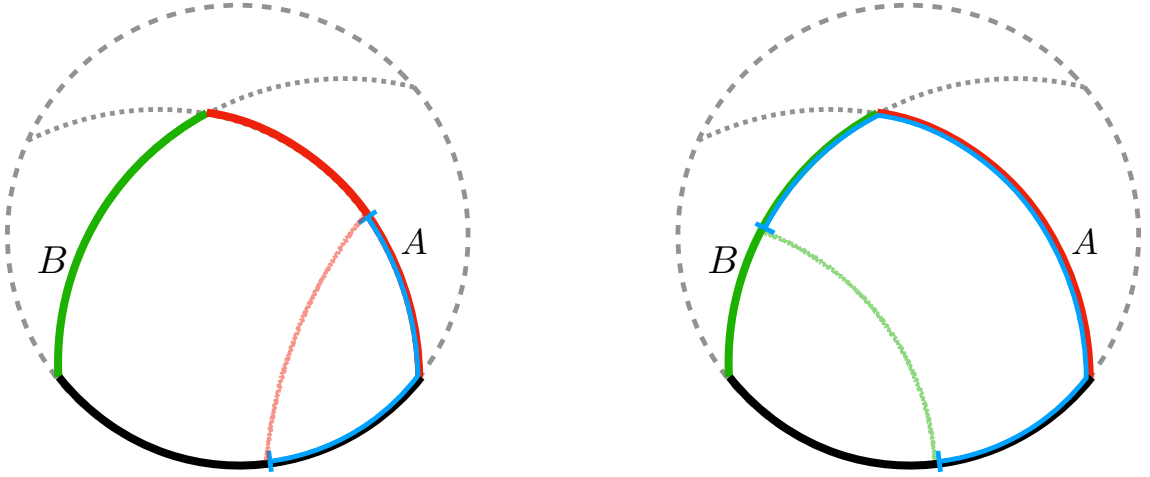


Figure 12: A pictorial representation of the quantum extremal surface in the double holographic interpretation of our model. The RT surfaces of the AdS/BCFT setup select the QES in the brane perspective. The phases A and B are depicted respectively on the left and on the right. In the B phase the QES selects a region which comprises the entire AdS_2 region associated with A and part of the interior of the AdS_2 region associated with B .

the interior of universe B .

Driving the system with a sequence of Hamiltonians

In our analysis we focused on quenching the system with one specific Hamiltonian. As discussed for instance in [77–80, 82, 97, 98] for the case of homogeneous boundary conditions, having an entire class of deformed Hamiltonian and a periodic behaviour allows for more complicated dynamical patterns. For finite θ , the system exhibits a periodic behaviour and gets revived to its initial state at the end of each period. One can then drive the system with a different Hamiltonian at the end of each time period in a Floquet-like manner. The simplest case here would be an evolution governed by two different Hamiltonians H_{k_1} and H_{k_2} at fixed θ , with n -cycles

$$U = \left(e^{-iH_{k_2}t_2} e^{-iH_{k_1}t_1} \right)^n \quad (6.1)$$

where H_{k_i} drives the system for a period $t_i = \frac{2L \cosh(2\theta)}{k_i}$.

Choosing appropriately the parameters of our setup, it would then be possible to engineer a variety of situations. For instance one could have a dynamics where a phase transition from phase A to B and back would happen for either, both or none the evolution intervals associated with H_{k_1} and H_{k_2} .

Generalizations

Our explicit analysis is limited to the case of holographic CFTs. Even though the complete set of conformal data is unknown, the holographic geometric construction in terms of EOW branes leads to consider arbitrary values for the boundary entropy. In turn this allows to always find a window of parameters where a transition occurs. In the case of rational CFTs, on the other hand, the boundary entropy can only take a finite number of values given by the g -functions [3, 4, 7, 8]. It would then be interesting to revisit our analysis for the rational case and see if this dynamical phase transition is linked to the irrational character of holographic CFTs, as it is the case for chaotic and scrambling behaviour (see, *e.g.*, [99–101]).

Also, we only considered the case where the interval is adjacent to one of the boundaries. An interval which does not include any of the boundaries will give rise to a more complicated pattern for the evolution of the entanglement entropy after the quench. An interesting observation that has been made for finite systems with periodic boundary conditions is that the SSD quench dynamics can be used to bring different initial states to a state where the entanglement entropy of an interval approximately matches that of the vacuum state at late times [36, 38].

Another interesting direction is extending the discussions to the thermal case. The relevant Euclidean CFT computation in this case is not on the infinite strip, but on the finite one with two sides identified, or equivalently on the annulus. Holographically it would correspond to considering an AdS black hole geometry with two branes selecting a part of the bulk. Despite a first principle CFT computation might be technically challenging in this case, the same techniques of section 5 would allow to conduct an holographic study. We hope to report on this in the future.

Acknowledgement

We thank Pawel Caputa, Yingfei Gu, Hosho Katsura, Masamichi Miyaji, Yu Nakayama, Dominik Neuenfeld, Tatsuma Nishioka, Jiaxin Qiao, Erik Tonni and Satoshi Yamaguchi for useful discussions and comments at various stages of this work, and especially Tadashi Takayanagi for comments on a draft of the paper. The authors are grateful for the hospitality of Galileo Galilei Institute for Theoretical Physics (GGI). AB and FG are grateful for the hospitality of Perimeter Institute where part of this work was carried out. DG thanks the University of Florence and INFN for partial support during the completion of this work, and IAS Tsinghua and YITP Kyoto where the work was partially presented. DG also thanks YITP for providing regular visiting opportunities.

DG is supported by Grant-in-Aid for Transformative Research Areas(A) “Extreme Universe” No. 21H05190. FG would like to thank the Isaac Newton Institute for Mathematical Sciences, Cambridge, for support and hospitality during the programme Black holes: bridges between number theory and holographic quantum information where work on this paper was undertaken. This research was supported in part by the Simons Foundation through the Simons Foundation Emmy Noether Fellows Program at Perimeter Institute. Research at Perimeter Institute is supported by the Government of Canada through the Department of Innovation, Science and Economic Development and by the Province of Ontario through the Ministry of Research, Innovation and Science. This work was also supported in part by EPSRC grant no EP/R014604/1.

A Stress tensor in the UHP

On the infinite strip of width L with conformal boundary conditions on the edges only one set of Virasoro symmetries survives. To see that, one can use the conformal map

$$z = e^{\frac{\pi}{L}w}, \quad w = \tau + i\sigma, \quad \sigma \in [0, L] \quad (\text{A.1})$$

to bring the strip to the UHP. See, *e.g.*, [3, 102].

In the UHP Virasoro generators are still defined in terms of the stress energy tensor, though its holomorphic part and anti-holomorphic part are no longer independent from each other. More precisely, they conformal boundary conditions imply $T(z) = \bar{T}(\bar{z})$ when $z = \bar{z}$, *i.e.*, on the real axis. One can analytically continue the holomorphic stress tensor to the lower half plane defining $T(z^*) = \bar{T}(z)$, where z in the UHP. Similarly for the anti-holomorphic part of the stress tensor $\bar{T}(z^*) = T(z)$.

Then the Virasoro generators can be expressed in the UHP in a similar way as in the full complex plane

$$L_n = \frac{1}{2\pi i} \oint_{C'} dz z^{n+1} T(z) - \frac{1}{2\pi i} \oint_{C'} dz^* z^{*n+1} \bar{T}(z) \quad (\text{A.2})$$

where the contour C' is a semicircle and a segment along the real axis including the origin. Using the analytic properties of the stress tensor this can also be expressed as a contour integral in the full complex plane

$$L_n = \frac{1}{2\pi i} \oint_C dz z^{n+1} T(z) = -\frac{1}{2\pi i} \oint_C d\bar{z} \bar{z}^{n+1} \bar{T}(\bar{z}) = \bar{L}_n, \quad (\text{A.3})$$

In the main text we will express the Virasoro generators as contour integrals in the full complex plane using the holomorphic part and use the short-hand notation

$$\oint z^{n+1} T(z) \equiv \frac{1}{2\pi i} \oint_C dz z^{n+1} T(z) = L_n. \quad (\text{A.4})$$

Notice that L_n now acts both on the holomorphic and anti-holomorphic coordinates of the bulk primary operator as

$$[L_n, \mathcal{O}(z, \bar{z})] = h(n+1)z^n \mathcal{O}(z, \bar{z}) + z^{n+1} \partial_z \mathcal{O}(z, \bar{z}) + \bar{h}(n+1)\bar{z}^n \mathcal{O}(z, \bar{z}) + \bar{z}^{n+1} \partial_{\bar{z}} \mathcal{O}(z, \bar{z}). \quad (\text{A.5})$$

References

- [1] J. L. Cardy, “Boundary Conditions, Fusion Rules and the Verlinde Formula,” Nucl. Phys. B **324** (1989), 581-596 doi:10.1016/0550-3213(89)90521-X
- [2] J. L. Cardy and D. C. Lewellen, “Bulk and boundary operators in conformal field theory,” Phys. Lett. B **259** (1991), 274-278 doi:10.1016/0370-2693(91)90828-E
- [3] J. L. Cardy, “Boundary conformal field theory,” [[arXiv:hep-th/0411189](#)].
- [4] I. Affleck and A. W. W. Ludwig, “Universal noninteger ‘ground state degeneracy’ in critical quantum systems,” Phys. Rev. Lett. **67** (1991), 161-164 doi:10.1103/PhysRevLett.67.161
- [5] P. Calabrese and J. L. Cardy, “Entanglement entropy and quantum field theory,” J. Stat. Mech. **0406** (2004), P06002 doi:10.1088/1742-5468/2004/06/P06002 [[arXiv:hep-th/0405152](#) [hep-th]].
- [6] P. Calabrese and J. Cardy, “Entanglement entropy and conformal field theory,” J. Phys. A **42** (2009), 504005 doi:10.1088/1751-8113/42/50/504005 [[arXiv:0905.4013](#) [cond-mat.stat-mech]].
- [7] R. E. Behrend, P. A. Pearce, V. B. Petkova and J. B. Zuber, “On the classification of bulk and boundary conformal field theories,” Phys. Lett. B **444** (1998), 163-166 doi:10.1016/S0370-2693(98)01374-4 [[arXiv:hep-th/9809097](#) [hep-th]].
- [8] R. E. Behrend, P. A. Pearce, V. B. Petkova and J. B. Zuber, “Boundary conditions in rational conformal field theories,” Nucl. Phys. B **570** (2000), 525-589 doi:10.1016/S0550-3213(99)00592-1 [[arXiv:hep-th/9908036](#) [hep-th]].
- [9] I. Heemskerk, J. Penedones, J. Polchinski and J. Sully, “Holography from Conformal Field Theory,” JHEP **10** (2009), 079 doi:10.1088/1126-6708/2009/10/079 [[arXiv:0907.0151](#) [hep-th]].

- [10] T. Hartman, C. A. Keller and B. Stoica, “Universal Spectrum of 2d Conformal Field Theory in the Large c Limit,” JHEP **09** (2014), 118 doi:10.1007/JHEP09(2014)118 [[arXiv:1405.5137](#) [hep-th]].
- [11] G. Penington, “Entanglement Wedge Reconstruction and the Information Paradox,” JHEP **09** (2020), 002 doi:10.1007/JHEP09(2020)002 [[arXiv:1905.08255](#) [hep-th]].
- [12] A. Almheiri, N. Engelhardt, D. Marolf and H. Maxfield, “The entropy of bulk quantum fields and the entanglement wedge of an evaporating black hole,” JHEP **12** (2019), 063 doi:10.1007/JHEP12(2019)063 [[arXiv:1905.08762](#) [hep-th]].
- [13] A. Almheiri, R. Mahajan, J. Maldacena and Y. Zhao, “The Page curve of Hawking radiation from semiclassical geometry,” JHEP **03** (2020), 149 doi:10.1007/JHEP03(2020)149 [[arXiv:1908.10996](#) [hep-th]].
- [14] A. Almheiri, T. Hartman, J. Maldacena, E. Shaghoulian and A. Tajdini, “Replica Wormholes and the Entropy of Hawking Radiation,” JHEP **05** (2020), 013 doi:10.1007/JHEP05(2020)013 [[arXiv:1911.12333](#) [hep-th]].
- [15] A. Almheiri, T. Hartman, J. Maldacena, E. Shaghoulian and A. Tajdini, “The entropy of Hawking radiation,” Rev. Mod. Phys. **93** (2021) no.3, 035002 doi:10.1103/RevModPhys.93.035002 [[arXiv:2006.06872](#) [hep-th]].
- [16] T. Takayanagi, “Holographic Dual of BCFT,” Phys. Rev. Lett. **107** (2011), 101602 doi:10.1103/PhysRevLett.107.101602 [[arXiv:1105.5165](#) [hep-th]].
- [17] M. Fujita, T. Takayanagi and E. Tonni, “Aspects of AdS/BCFT,” JHEP **11** (2011), 043 doi:10.1007/JHEP11(2011)043 [[arXiv:1108.5152](#) [hep-th]].
- [18] H. Kanda, M. Sato, Y. k. Suzuki, T. Takayanagi and Z. Wei, “AdS/BCFT with brane-localized scalar field,” JHEP **03** (2023), 105 doi:10.1007/JHEP03(2023)105 [[arXiv:2302.03895](#) [hep-th]].
- [19] K. Suzuki, Y. k. Suzuki, T. Tsuda and M. Watanabe, “Information metric on the boundary,” JHEP **05** (2023), 013 doi:10.1007/JHEP05(2023)013 [[arXiv:2212.10899](#) [hep-th]].
- [20] H. Kanda, T. Kawamoto, Y. k. Suzuki, T. Takayanagi, K. Tasuki and Z. Wei, “Entanglement Phase Transition in Holographic Pseudo Entropy,” [[arXiv:2311.13201](#) [hep-th]].

- [21] M. Miyaji and C. Murdia, “Holographic BCFT with a Defect on the End-of-the-World brane,” JHEP **11** (2022), 123 doi:10.1007/JHEP11(2022)123 [[arXiv:2208.13783](#) [hep-th]].
- [22] S. Biswas, J. Kastikainen, S. Shashi and J. Sully, “Holographic BCFT spectra from brane mergers,” JHEP **11** (2022), 158 doi:10.1007/JHEP11(2022)158 [[arXiv:2209.11227](#) [hep-th]].
- [23] H. Geng, S. Lüster, R. K. Mishra and D. Wakeham, “Holographic BCFTs and Communicating Black Holes,” jhep **08** (2021), 003 doi:10.1007/JHEP08(2021)003 [[arXiv:2104.07039](#) [hep-th]].
- [24] M. Miyaji, T. Takayanagi and T. Ugajin, “Spectrum of End of the World Branes in Holographic BCFTs,” JHEP **06** (2021), 023 doi:10.1007/JHEP06(2021)023 [[arXiv:2103.06893](#) [hep-th]].
- [25] W. Reeves, M. Rozali, P. Simidzija, J. Sully, C. Waddell and D. Wakeham, “Looking for (and not finding) a bulk brane,” JHEP **12** (2021), 002 doi:10.1007/JHEP12(2021)002 [[arXiv:2108.10345](#) [hep-th]].
- [26] J. Sully, M. Van Raamsdonk and D. Wakeham, “BCFT entanglement entropy at large central charge and the black hole interior,” JHEP **03** (2021), 167 doi:10.1007/JHEP03(2021)167 [[arXiv:2004.13088](#) [hep-th]].
- [27] M. Rozali, J. Sully, M. Van Raamsdonk, C. Waddell and D. Wakeham, “Information radiation in BCFT models of black holes,” JHEP **05** (2020), 004 doi:10.1007/JHEP05(2020)004 [[arXiv:1910.12836](#) [hep-th]].
- [28] P. Caputa, T. Numasawa, T. Shimaji, T. Takayanagi and Z. Wei, “Double Local Quenches in 2D CFTs and Gravitational Force,” JHEP **09** (2019), 018 doi:10.1007/JHEP09(2019)018 [[arXiv:1905.08265](#) [hep-th]].
- [29] L. Bianchi, S. De Angelis and M. Meineri, “Radiation, entanglement and islands from a boundary local quench,” SciPost Phys. **14** (2023) no.6, 148 doi:10.21468/SciPostPhys.14.6.148 [[arXiv:2203.10103](#) [hep-th]].
- [30] A. Gendiar, R. Krcmar and T. Nishino, “Spherical Deformation for One-Dimensional Quantum Systems,” Prog. Theor. Phys. **122** (2009) no.4, 953–967 [erratum: Prog. Theor. Phys. **123** (2010), 393] doi:10.1143/PTP.122.953 [[arXiv:0810.0622](#) [cond-mat.str-el]].

- [31] A. Gendiar, M. Daniška, Y. Lee, and T. Nishino, “Suppression of finite-size effects in one-dimensional correlated system,” *Phys. Rev. A* **83** (2011), 052118 doi:10.1103/PhysRevA.83.052118 [[arXiv:1012.1472](#) [cond-mat]].
- [32] T. Hikihara and T. Nishino, “Connecting distant ends of one-dimensional critical systems by a sine-square deformation,” *Phys. Rev. B* **83** (2011) no.6, 060414 doi:10.1103/physrevb.83.060414 [[arXiv:1012.0472](#) [cond-mat]].
- [33] H. Katsura, “Sine-square deformation of solvable spin chains and conformal field theories,” *J. Phys. A* **45** (2012), 115003 doi:10.1088/1751-8113/45/11/115003 [[arXiv:1110.2459](#) [cond-mat.stat-mech]].
- [34] K. Okunishi, “Sine-square deformation and Möbius quantization of 2D conformal field theory,” *PTEP* **2016** (2016) no.6, 063A02 doi:10.1093/ptep/ptw060 [[arXiv:1603.09543](#) [hep-th]].
- [35] X. Wen, S. Ryu and A. W. W. Ludwig, “Evolution operators in conformal field theories and conformal mappings: Entanglement Hamiltonian, the sine-square deformation, and others,” *Phys. Rev. B* **93** (2016) no.23, 235119 doi:10.1103/PhysRevB.93.235119 [[arXiv:1604.01085](#) [cond-mat.str-el]].
- [36] K. Goto, M. Nozaki, K. Tamaoka, M. T. Tan and S. Ryu, “Non-Equilibrating a Black Hole with Inhomogeneous Quantum Quench,” [[arXiv:2112.14388](#) [hep-th]].
- [37] K. Goto, M. Nozaki, S. Ryu, K. Tamaoka and M. T. Tan, “Scrambling and Recovery of Quantum Information in Inhomogeneous Quenches in Two-dimensional Conformal Field Theories,” [[arXiv:2302.08009](#) [hep-th]].
- [38] M. Nozaki, K. Tamaoka and M. T. Tan, “Inhomogeneous quenches as state preparation in two-dimensional conformal field theories,” [[arXiv:2310.19376](#) [hep-th]].
- [39] H. Katsura, “Exact ground state of the sine-square deformed XY spin chain,” *J. Phys. A* **44** (2011) no.25, 252001 doi:10.1088/1751-8113/44/25/252001 [[arXiv:1104.1721](#) [cond-mat.stat-mech]].
- [40] N. Shibata and C. Hotta, “Boundary effects in the density-matrix renormalization group calculation,” *Phys. Rev. B* **84** (2011) no.11, 115116 doi:10.1103/physrevb.84.115116 [[arXiv:1106.6202](#) [cond-mat.str-el]].
- [41] I. Maruyama, H. Katsura and T. Hikihara, “Sine-square deformation of free fermion systems in one and higher dimensions,” doi:10.1103/PhysRevB.84.165132 [[arXiv:1108.2973](#) [cond-mat.stat-mech]].

- [42] T. Tada, “Sine-Square Deformation and its Relevance to String Theory,” *Mod. Phys. Lett. A* **30** (2015) no.19, 1550092 doi:10.1142/S0217732315500923 [[arXiv:1404.6343](#) [hep-th]].
- [43] N. Ishibashi and T. Tada, “Infinite circumference limit of conformal field theory,” *J. Phys. A* **48** (2015) no.31, 315402 doi:10.1088/1751-8113/48/31/315402 [[arXiv:1504.00138](#) [hep-th]].
- [44] N. Ishibashi and T. Tada, “Dipolar quantization and the infinite circumference limit of two-dimensional conformal field theories,” *Int. J. Mod. Phys. A* **31** (2016) no.32, 1650170 doi:10.1142/S0217751X16501700 [[arXiv:1602.01190](#) [hep-th]].
- [45] I. Affleck, “Boundary condition changing operators in conformal field theory and condensed matter physics,” *Nucl. Phys. B Proc. Suppl.* **58** (1997), 35-41 doi:10.1016/S0920-5632(97)00411-8 [[arXiv:hep-th/9611064](#) [hep-th]].
- [46] P. Calabrese and J. L. Cardy, “Evolution of entanglement entropy in one-dimensional systems,” *J. Stat. Mech.* **0504** (2005), P04010 doi:10.1088/1742-5468/2005/04/P04010 [[arXiv:cond-mat/0503393](#) [cond-mat]].
- [47] X. Wen and J. Q. Wu, “Quantum dynamics in sine-square deformed conformal field theory: Quench from uniform to nonuniform conformal field theory,” *Phys. Rev. B* **97** (2018) no.18, 184309 doi:10.1103/PhysRevB.97.184309 [[arXiv:1802.07765](#) [cond-mat.str-el]].
- [48] D. C. Lewellen, “Sewing constraints for conformal field theories on surfaces with boundaries,” *Nucl. Phys. B* **372** (1992), 654-682 doi:10.1016/0550-3213(92)90370-Q
- [49] T. Hartman, “Entanglement Entropy at Large Central Charge,” [[arXiv:1303.6955](#) [hep-th]].
- [50] A. L. Fitzpatrick, J. Kaplan and M. T. Walters, “Universality of Long-Distance AdS Physics from the CFT Bootstrap,” *JHEP* **08** (2014), 145 doi:10.1007/JHEP08(2014)145 [[arXiv:1403.6829](#) [hep-th]].
- [51] P. Caputa, J. Simón, A. Štikonas and T. Takayanagi, “Quantum Entanglement of Localized Excited States at Finite Temperature,” *JHEP* **01** (2015), 102 doi:10.1007/JHEP01(2015)102 [[arXiv:1410.2287](#) [hep-th]].

- [52] C. T. Asplund, A. Bernamonti, F. Galli and T. Hartman, “Holographic Entanglement Entropy from 2d CFT: Heavy States and Local Quenches,” JHEP **02** (2015), 171 doi:10.1007/JHEP02(2015)171 [[arXiv:1410.1392](#) [hep-th]].
- [53] V. Balasubramanian, A. Bernamonti, B. Craps, T. De Jonckheere and F. Galli, “Heavy-Heavy-Light-Light correlators in Liouville theory,” JHEP **08** (2017), 045 doi:10.1007/JHEP08(2017)045 [[arXiv:1705.08004](#) [hep-th]].
- [54] E. Perlmutter, “Virasoro conformal blocks in closed form,” JHEP **08** (2015), 088 doi:10.1007/JHEP08(2015)088 [[arXiv:1502.07742](#) [hep-th]].
- [55] A. L. Fitzpatrick, J. Kaplan and M. T. Walters, “Virasoro Conformal Blocks and Thermalities from Classical Background Fields,” JHEP **11** (2015), 200 doi:10.1007/JHEP11(2015)200 [[arXiv:1501.05315](#) [hep-th]].
- [56] T. Anous, T. Hartman, A. Rovai and J. Sonner, “Black Hole Collapse in the $1/c$ Expansion,” JHEP **07** (2016), 123 doi:10.1007/JHEP07(2016)123 [[arXiv:1603.04856](#) [hep-th]].
- [57] S. Ryu and T. Takayanagi, “Holographic derivation of entanglement entropy from AdS/CFT,” Phys. Rev. Lett. **96** (2006), 181602 doi:10.1103/PhysRevLett.96.181602 [[arXiv:hep-th/0603001](#) [hep-th]].
- [58] V. E. Hubeny, M. Rangamani and T. Takayanagi, “A Covariant holographic entanglement entropy proposal,” JHEP **07** (2007), 062 doi:10.1088/1126-6708/2007/07/062 [[arXiv:0705.0016](#) [hep-th]].
- [59] I. Akal, Y. Kusuki, T. Takayanagi and Z. Wei, “Codimension two holography for wedges,” Phys. Rev. D **102** (2020) no.12, 126007 doi:10.1103/PhysRevD.102.126007 [[arXiv:2007.06800](#) [hep-th]].
- [60] Al. B. Zamolodchikov, “Conformal symmetry in two-dimensional space: an explicit recurrence formula for the conformal partial wave amplitude,” Commun. Math. Phys. **96** (1984), 419-422 doi:10.1007/BF01214585
- [61] Al. B. Zamolodchikov, “Conformal symmetry in two-dimensional space: Recursion representation of conformal block,” Theor. Math. Phys. **73** (1987) 1088.
- [62] M. Headrick, “Entanglement Renyi entropies in holographic theories,” Phys. Rev. D **82** (2010), 126010 doi:10.1103/PhysRevD.82.126010 [[arXiv:1006.0047](#) [hep-th]].

- [63] S. Sotiriadis and J. Cardy, “Inhomogeneous Quantum Quenches,” *J. Stat. Mech.* **0811** (2008), P11003 doi:10.1088/1742-5468/2008/11/P11003 [[arXiv:0808.0116](#) [cond-mat.stat-mech]].
- [64] P. Calabrese and J. Cardy, “Quantum quenches in 1 + 1 dimensional conformal field theories,” *J. Stat. Mech.* **1606** (2016) no.6, 064003 doi:10.1088/1742-5468/2016/06/064003 [[arXiv:1603.02889](#) [cond-mat.stat-mech]].
- [65] J. Dubail, J. M. Stéphan, J. Viti and P. Calabrese, “Conformal field theory for inhomogeneous one-dimensional quantum systems: the example of non-interacting Fermi gases,” *SciPost Phys.* **2** (2017) no.1, 002 doi:10.21468/SciPostPhys.2.1.002 [[arXiv:1606.04401](#) [cond-mat.str-el]].
- [66] V. Alba, B. Bertini, M. Fagotti, L. Piroli and P. Ruggiero, “Generalized-hydrodynamic approach to inhomogeneous quenches: correlations, entanglement and quantum effects,” *J. Stat. Mech.* **2111** (2021), 114004 doi:10.1088/1742-5468/ac257d [[arXiv:2104.00656](#) [cond-mat.stat-mech]].
- [67] D. Horvath, S. Sotiriadis, M. Kormos and G. Takacs, “Inhomogeneous quantum quenches in the sine-Gordon theory,” *SciPost Phys.* **12** (2022) no.5, 144 doi:10.21468/SciPostPhys.12.5.144 [[arXiv:2109.06869](#) [cond-mat.str-el]].
- [68] V. Balasubramanian, A. Bernamonti, J. de Boer, B. Craps, L. Franti, F. Galli, E. Keski-Vakkuri, B. Müller and A. Schäfer, “Inhomogeneous holographic thermalization,” *JHEP* **10** (2013), 082 doi:10.1007/JHEP10(2013)082 [[arXiv:1307.7086](#) [hep-th]].
- [69] V. Balasubramanian, A. Bernamonti, J. de Boer, B. Craps, L. Franti, F. Galli, E. Keski-Vakkuri, B. Müller and A. Schäfer, “Inhomogeneous Thermalization in Strongly Coupled Field Theories,” *Phys. Rev. Lett.* **111** (2013), 231602 doi:10.1103/PhysRevLett.111.231602 [[arXiv:1307.1487](#) [hep-th]].
- [70] K. A. Sohrobi, “Inhomogeneous Thermal Quenches,” *Phys. Rev. D* **96** (2017) no.2, 026012 doi:10.1103/PhysRevD.96.026012 [[arXiv:1509.00245](#) [hep-th]].
- [71] T. De Jonckheere and J. Lindgren, “Entanglement entropy in inhomogeneous quenches in $\text{AdS}_3/\text{CFT}_2$,” *Phys. Rev. D* **98** (2018) no.10, 106006 doi:10.1103/PhysRevD.98.106006 [[arXiv:1803.04718](#) [hep-th]].

- [72] X. Liu, A. McDonald, T. Numasawa, B. Lian and S. Ryu, “Quantum Quenches of Conformal Field Theory with Open Boundary,” [[arXiv:2309.04540](#) [cond-mat.stat-mech]].
- [73] P. Moosavi, “Inhomogeneous Conformal Field Theory Out of Equilibrium,” *Annales Henri Poincaré* **25** (2024) no.1, 1083-1122 doi:10.1007/s00023-021-01118-0 [[arXiv:1912.04821](#) [math-ph]].
- [74] E. Witten, “Coadjoint Orbits of the Virasoro Group,” *Commun. Math. Phys.* **114** (1988), 1 doi:10.1007/BF01218287
- [75] P. Caputa and D. Ge, “Entanglement and geometry from subalgebras of the Virasoro algebra,” *JHEP* **06** (2023), 159 doi:10.1007/JHEP06(2023)159 [[arXiv:2211.03630](#) [hep-th]].
- [76] D. Liska, V. Gritsev, W. Vleeshouwers and J. Minář, “Holographic Quantum Scars,” *SciPost Phys.* **15** (2023), 106 doi:10.21468/SciPostPhys.15.3.106 [[arXiv:2212.05962](#) [hep-th]].
- [77] X. Wen and J. Q. Wu, “Floquet conformal field theory,” [[arXiv:1805.00031](#) [cond-mat.str-el]].
- [78] X. Wen, R. Fan, A. Vishwanath and Y. Gu, “Periodically, quasiperiodically, and randomly driven conformal field theories,” *Phys. Rev. Res.* **3** (2021) no.2, 023044 doi:10.1103/PhysRevResearch.3.023044 [[arXiv:2006.10072](#) [cond-mat.stat-mech]].
- [79] R. Fan, Y. Gu, A. Vishwanath and X. Wen, “Floquet conformal field theories with generally deformed Hamiltonians,” *SciPost Phys.* **10** (2021) no.2, 049 doi:10.21468/SciPostPhys.10.2.049 [[arXiv:2011.09491](#) [hep-th]].
- [80] X. Wen, Y. Gu, A. Vishwanath and R. Fan, “Periodically, Quasi-periodically, and Randomly Driven Conformal Field Theories (II): Furstenberg’s Theorem and Exceptions to Heating Phases,” *SciPost Phys.* **13** (2022) no.4, 082 doi:10.21468/SciPostPhys.13.4.082 [[arXiv:2109.10923](#) [cond-mat.stat-mech]].
- [81] G. Grimaldi, J. Hernandez and R. C. Myers, “Quantum extremal islands made easy. Part IV. Massive black holes on the brane,” *JHEP* **03** (2022), 136 doi:10.1007/JHEP03(2022)136 [[arXiv:2202.00679](#) [hep-th]].
- [82] H. Jiang and M. Mezei, “New horizons for inhomogeneous quenches and Floquet CFT,” [[arXiv:2404.07884](#) [hep-th]].

- [83] M. Banados, “Three-dimensional quantum geometry and black holes,” AIP Conf. Proc. **484** (1999) no.1, 147-169 doi:10.1063/1.59661 [[arXiv:hep-th/9901148](#) [hep-th]].
- [84] M. M. Roberts, “Time evolution of entanglement entropy from a pulse,” JHEP **12** (2012), 027 doi:10.1007/JHEP12(2012)027 [[arXiv:1204.1982](#) [hep-th]].
- [85] P. Caputa and J. M. Magan, “Quantum Computation as Gravity,” Phys. Rev. Lett. **122** (2019) no.23, 231302 doi:10.1103/PhysRevLett.122.231302 [[arXiv:1807.04422](#) [hep-th]].
- [86] J. Erdmenger, M. Flory, M. Gerbershagen, M. P. Heller and A. L. Weigel, “Exact Gravity Duals for Simple Quantum Circuits,” SciPost Phys. **13** (2022) no.3, 061 doi:10.21468/SciPostPhys.13.3.061 [[arXiv:2112.12158](#) [hep-th]].
- [87] T. Hartman and J. Maldacena, “Time Evolution of Entanglement Entropy from Black Hole Interiors,” JHEP **05** (2013), 014 doi:10.1007/JHEP05(2013)014 [[1303.1080](#) [hep-th]].
- [88] C. T. Asplund and A. Bernamonti, “Mutual information after a local quench in conformal field theory,” Phys. Rev. D **89** (2014) no.6, 066015 doi:10.1103/PhysRevD.89.066015 [[arXiv:1311.4173](#) [hep-th]].
- [89] L. Randall and R. Sundrum, “A Large mass hierarchy from a small extra dimension,” Phys. Rev. Lett. **83** (1999), 3370-3373 doi:10.1103/PhysRevLett.83.3370 [[arXiv:hep-ph/9905221](#) [hep-ph]].
- [90] L. Randall and R. Sundrum, “An Alternative to compactification,” Phys. Rev. Lett. **83** (1999), 4690-4693 doi:10.1103/PhysRevLett.83.4690 [[arXiv:hep-th/9906064](#) [hep-th]].
- [91] A. Karch and L. Randall, “Locally localized gravity,” JHEP **05** (2001), 008 doi:10.1088/1126-6708/2001/05/008 [[arXiv:hep-th/0011156](#) [hep-th]].
- [92] N. Engelhardt and A. C. Wall, “Quantum Extremal Surfaces: Holographic Entanglement Entropy beyond the Classical Regime,” JHEP **01** (2015), 073 doi:10.1007/JHEP01(2015)073 [[arXiv:1408.3203](#) [hep-th]].
- [93] H. Geng and A. Karch, “Massive islands,” JHEP **09** (2020), 121 doi:10.1007/JHEP09(2020)121 [[arXiv:2006.02438](#) [hep-th]].

- [94] H. Z. Chen, R. C. Myers, D. Neuenfeld, I. A. Reyes and J. Sandor, “Quantum Extremal Islands Made Easy, Part I: Entanglement on the Brane,” JHEP **10** (2020), 166 doi:10.1007/JHEP10(2020)166 [[arXiv:2006.04851](#) [hep-th]].
- [95] H. Z. Chen, R. C. Myers, D. Neuenfeld, I. A. Reyes and J. Sandor, “Quantum Extremal Islands Made Easy, Part II: Black Holes on the Brane,” JHEP **12** (2020), 025 doi:10.1007/JHEP12(2020)025 [[arXiv:2010.00018](#) [hep-th]].
- [96] H. Geng, A. Karch, C. Perez-Pardavila, S. Raju, L. Randall, M. Riojas and S. Shashi, “Information Transfer with a Gravitating Bath,” SciPost Phys. **10** (2021) no.5, 103 doi:10.21468/SciPostPhys.10.5.103 [[arXiv:2012.04671](#) [hep-th]].
- [97] B. Lapierre, K. Choo, C. Tauber, A. Tiwari, T. Neupert and R. Chitra, “Emergent black hole dynamics in critical Floquet systems,” Phys. Rev. Res. **2** (2020) no.2, 023085 doi:10.1103/PhysRevResearch.2.023085 [[arXiv:1909.08618](#) [cond-mat.str-el]].
- [98] B. Lapierre and P. Moosavi, “Geometric approach to inhomogeneous Floquet systems,” Phys. Rev. B **103** (2021), 224303 doi:10.1103/PhysRevB.103.224303 [[arXiv:2010.11268](#) [cond-mat.stat-mech]].
- [99] D. A. Roberts and D. Stanford, “Two-dimensional conformal field theory and the butterfly effect,” Phys. Rev. Lett. **115** (2015) no.13, 131603 doi:10.1103/PhysRevLett.115.131603 [[arXiv:1412.5123](#) [hep-th]].
- [100] C. T. Asplund, A. Bernamonti, F. Galli and T. Hartman, “Entanglement Scrambling in 2d Conformal Field Theory,” JHEP **09** (2015), 110 doi:10.1007/JHEP09(2015)110 [[arXiv:1506.03772](#) [hep-th]].
- [101] P. Hosur, X. L. Qi, D. A. Roberts and B. Yoshida, “Chaos in quantum channels,” JHEP **02** (2016), 004 doi:10.1007/JHEP02(2016)004 [[arXiv:1511.04021](#) [hep-th]].
- [102] P. Di Francesco, P. Mathieu and D. Senechal, “Conformal Field Theory,” Springer-Verlag, 1997, ISBN 978-0-387-94785-3, 978-1-4612-7475-9 doi:10.1007/978-1-4612-2256-9